Spectrum of BDNF expression changes and reactive glial phenotypes across brain regions precede neuronal loss and predict therapeutic effects of BDNF in early stages of SCA1

Abbreviated title: Brain wide SCA1 pathology and effects of BDNF

Juao-Guilherme Rosa[1], Katherine Hamel[1], Carrie Sheeler[1], Ella Borgenheimer[1], Stephen Gilliat[1], Alyssa Soles[1], Fares Ghannoum[1], Kaelin Sbrocco[1], Colleen Forster[4], Orion Rainwater[3], Harry Orr[2, 3], Marija Cvetanovic[1,2*]

1. Department of Neuroscience,
2. Institute for Translational Neuroscience, University of Minnesota 2101 6th Street SE, Minneapolis, MN 55455
3. Department of Lab Medicine and Pathology
4. BLS Histology and IHC Laboratory

Corresponding Author:

Marija Cvetanovic, Department of Neuroscience, University of Minnesota

2101 6th Street SE, Minneapolis, MN 55455

E-mail: mcvetano@umn.edu

Tel. 612-626-4918

Abstract (319 words)

Spinocerebellar ataxia type 1 (SCA1) is a progressive neurodegenerative disease caused by an abnormal expansion of CAG repeats in the gene *Ataxin1* (*ATXN1*) and characterized by motor deficits, cognitive decline, and premature lethality. Due to the severe cerebellar degeneration seen in SCA1, the pathogenesis of Purkinje cells has been the main focus of previous studies. However, mutant ATXN1 is expressed throughout the brain, and pathology in brain regions beyond the cerebellar cortex likely contributes to the symptoms of SCA1. Here, using immunohistochemistry and gene expression analysis we investigated early-stage SCA1 alterations in neurons, astrocytes, and microglia in clinically relevant SCA1 brain regions including the cerebellum, medulla oblongata, hippocampus, and motor cortex of *Atxn1*$^{154Q/2Q}$ mice, a knock-in mouse model of SCA1 expressing mutant ATXN1 broadly.

Our results indicate a spectrum of astrocyte and microglial phenotypes across brain regions early in SCA1. We found reduced expression of homeostatic astrocytic genes *Kcnj10*, *Aqp4*, *Slc1a2* and *Gja1* in 12 week old *Atxn1*$^{154Q/2Q}$ mice, all of which are key for neuronal function, in the hippocampus and medulla. At the same age, the expression of these genes was increased in the cortex, indicating region-specific astrocyte reactive phenotypes. We have found altered microglial density throughout the brain, with decreases in cerebellar white matter but increases in medulla, motor cortex and corpus callosum. On the other hand, neuronal pathology was evident only in cerebellar Purkinje cells at this early stage of SCA1.

We have previously shown that expression of brain-derived neurotrophic factor (BDNF), an astrocyte-released growth factor important for the survival and function of neurons, is reduced in the cerebellum, and exogenous BDNF treatment has therapeutic potential for cerebellar aspects of disease in Purkinje cells specific transgenic mouse model of SCA1 (*Pcp2-ATXN1[82Q]* line).

We report here that BDNF expression is decreased in the cerebellar Bergmann glia of patients with SCA1.

Moreover, we found brain region specific changes in BDNF expression in *Atxn1*$^{154Q/2Q}$ *mice* with decreased expression in the cerebellum and hippocampus, and increased expression in the medulla and cortex. Using ALZET pumps to deliver BDNF, we have found that BDNF treatment ameliorated several aspects of SCA1 pathogenesis, including motor deficits, learning and problem-solving strategy development, hippocampal neurogenesis, and expression of astrocyte homeostatic genes in the hippocampus.

Introduction

Spinocerebellar ataxia type-1 (SCA1) is an inherited neurodegenerative disorder caused by CAG repeat expansions in the *Ataxin-1* (*ATXN1)* gene. Repeat expansions of about 39 or more CAG repeats result in the expression of a toxic polyglutamine (polyQ) ATXN1 protein [1]. SCA1 is characterized by progressive degeneration that is most severe in the cerebellum and brainstem, but is present in other brain regions as well, and manifests behaviorally as deficits in motor coordination (i.e. ataxia), swallowing, speaking, cognition, and mood [2][3][4]. While *Atxn1*-targeting antisense oligonucleotides (ASOs) show promise in pre-clinical trials [5], there are currently no disease-modifying treatments available for SCA1.

Motor deficits and underlying cerebellar pathology have been the focus of the majority of SCA1 studies so far. However, *ATXN1* is expressed throughout the brain and likely affects brain regions beyond the cerebellum [6][7]. While extra-cerebellar pathology in SCA1 patients remains less understood, it is described in brain stem, motor cortex and hippocampus and is thought to contribute to SCA1 symptoms such as cognitive deficits, mood disorders, difficulties in respiration and swallowing, and premature lethality [8][9][10][11][12][13]. To better understand brain-wide SCA1 pathology and therapeutic potential of BDNF for SCA1, we have utilized the

Atxn1$^{154Q/2Q}$ mouse model of SCA1 wherein 154 CAG repeats have been knocked-in into the endogenous mouse *Atxn1* gene [14]. Because the *Atxn1* gene is expressed under the endogenous promoter, *Atxn1*$^{154Q/2Q}$ mice express polyQ ATXN1 in neuronal and non-neuronal cells throughout the central nervous system and peripheral tissues. As a result, in addition to motor deficits, the *Atxn1*$^{154Q/2Q}$ mice exhibit a premature lethality, failure to gain weight, and cognitive deficits [14][15]. Furthermore, there is evidence of extra-cerebellar pathology in *Atxn1*$^{154Q/2Q}$ mice, although it remains to be thoroughly characterized [14][16][17].

Therefore, we performed a comparative characterization of BDNF expression, neuronal and glial pathology in the cerebellum, medulla, hippocampus, and motor cortex of 12 week old *Atxn1*$^{154Q/2Q}$ mice. We found a spectrum of brain region specific changes in BDNF expression, and in astrocyte and microglial phenotypes. Hippocampus and medulla had a significant decrease in the expression of astrocytic genes *Kcnj10*, *Aqp4*, *Slc1a2* and *Gja1* that play a critical role in the maintenance of brain homeostasis by regulating local concentrations of potassium (*Kir4.1*), water (*Aqp4*), and glutamate (*Slc1a2*)[18][19][20][21]. On the other hand, expression of these genes was increased in the cortex of 12 week old *Atxn1*$^{154Q/2Q}$ mice. These astrocytic changes were accompanied by a decreased microglial density in cerebellar white matter, while microglial density was increased in medulla, motor cortex and underlying corpus callosum.

We previously showed that reactive NF-κB signaling regulates BDNF expression in the cerebellar astrocytes of *Pcp2-ATXN1[82Q]* mice and that chronic administration of exogenous BDNF into the lateral ventricle delayed the onset of motor deficits and development of cerebellar pathology in pre-symptomatic *Pcp2-ATXN1[82Q]* mice [22]. Further, chronic administration of exogenous BDNF ameliorated motor deficits and cerebellar pathology in symptomatic *Pcp2-ATXN1[82Q]* mice [23]. As these findings from the transgenic *Pcp2-ATXN1[82Q]* mouse model indicated that the BDNF expression is disrupted in SCA1 and may be a therapeutic target to treat SCA1, we asked whether BDNF expression is altered in cerebellar astrocytes in patients

with SCA1. We found a significant decrease in BDNF expression in cerebellar astrocytes of patients with SCA1 compared to their age and sex matched unaffected controls. Moreover, we found that in 12 week old *Atxn1*$^{154Q/2Q}$ mice, BDNF also showed a brain –region specific change in the expression, with decreased expression in the cerebellum and hippocampus and increased expression in the medulla and cortex.

We then tested the therapeutic efficacy of chronic delivery of BDNF on SCA1-like phenotypes, including motor and cognitive deficits, neuronal and glial pathology across brain regions, and reduced hippocampal neurogenesis. We found significant beneficial effect of BDNF on several SCA1-like phenotypes, including motor and cognitive deficits, hippocampal neurogenesis and astrocytic gene expression that was most significant in the hippocampus.

Materials and Methods

Mice

The creation of the *Atxn1*$^{154Q/2Q}$ mice was previously described [14]. Because repeat length in trinucleotide repeat expansions is unstable and prone to further expansion [24], we routinely perform genetic sequencing of our mouse lines. We found that the number of repeats has recently expanded in our colony from 154 CAG to 166 CAG. Based on previous studies this increase in CAG repeat number is expected to increase severity of disease and lower age of symptom onset. Equal number of male and female *Atxn1*$^{154Q/2Q}$and wild-type (WT) mice were randomly allocated to BDNF or control artificial cerebrospinal fluid (aCSF) groups (N = 10-12). We surgically implanted ALZET pumps (Alzet Model 1004) into 7-week-old mice in a subcutaneous pocket in their back. A delivery cannula was placed into the right lateral ventricle using stereotaxic surgery (A/P, 1.1 mm; M/L, 0.5 mm; D/V, –2.5 mm from Bregma) as previously described [6]. ALZET pumps delivered BDNF or aCSF at a steady flow rate for 4 weeks following implantation (20 µg of human recombinant BDNF (R&D Systems Cat. 248-BD-250/CF)

in 100µl per micropump, resulting in a delivery rate of 0.71 µg/day) [23].

In all experiments, investigators were blinded to the genotype/treatment. While we started with the same number of animals in each group, the final number of animals per condition varied depending on the success of surgery, including survival from surgery and correct placement of the cannula. Five mice died (two female WT mice treated with aCSF and BDNF, one female and two male *Atxn1*$^{154Q/2Q}$ mice treated with BDNF). All mice were subjected to postmortem examination and this examination revealed that the cannula was correctly placed and was not obstructed in any of the mice.

Animal experimentation was approved by Institutional Animal Care and Use Committee (IACUC) of University of Minnesota and was conducted in accordance with the National Institutes of Health's (NIH) Principles of Laboratory Animal Care (86–23, revised 1985), and the American Physiological Society's Guiding Principles in the Use of Animals [25].

Cognitive testing

Mice were subjected to contextual fear conditioning prior to BDNF delivery (6 weeks of age). Mice were also tested via Barnes maze and re-tested on the contextual fear conditioning task 3 weeks after BDNF delivery started (10 weeks of age). Both cognitive tests were administered as previously done and are described below [15].

Sample sizes in the behavioral tests were determined using power analysis and prior experience with these tests, or previous reports using similar methodology. Experimenters were blinded to genotype and, where applicable, treatment during all tests.

Barnes maze. The maze was a white circular platform 91 cm in diameter with 20 5-cm circular holes spaced evenly around the edge, raised approximately 92 cm above the floor. One of the holes led to a 5 cm wide x 11 cm long x 5 cm deep opaque box (the "escape box") and the other 19 were covered. The testing room had visual cues on the walls to serve as landmarks, and all objects in the room were kept in the same places for every trial. The position of each mouse

was tracked using AnyMaze software. Mice were exposed to the maze for four 3-minute trials per day during four consecutive training days (intertrial interval of approximately 15 minutes). Mice which did not enter the escape box within 3 minutes were gently guided to it. Training day data is reported as a path length (distance traveled before entering the escape hole) and analyzed by two-way repeated measures ANOVA. A probe test was conducted 24 hours after the last training session. For the probe test, the escape hole was covered, and each mouse was allowed to explore the maze freely for 90 seconds. The time spent in each quadrant of the maze was recorded, and the amount of time spent in the goal quadrant (the quadrant centered on the goal hole) was analyzed by one-way ANOVA.

Search strategies on the training days were automatically classified and assigned cognitive scores using the Barnes maze unbiased strategy (BUNS) classification tool as described by Illouz *et al.* [26]. In order to compare learning rates between groups, cognitive scores for each mouse on each of the 16 training trials were plotted in GraphPad Prism 7.0. Linear regression was performed for each group and the slopes and elevations of the lines were compared using Prism's Analysis function.

Contextual fear conditioning. Conditioning took place in chambers with a floor consisting of stainless-steel rods through which shocks were delivered (Med Associates #ENV-008-FPU-M). On day 1, mice were placed in the chambers for a 10-minute period during which they received five foot shocks (0.70 mA, 2-second duration). Freezing during the 60 seconds after each shock was quantified automatically using VideoFreeze software (freezing was defined as a motion index ≤15 lasting ≥500 ms). 24 hours after the initial conditioning, mice were returned to the same chambers with the shock generators turned off and freezing behavior was monitored for 3 minutes. 1-2 hours after being placed in the conditioned context, mice were placed in a second context [the same chambers but different floor texture (smooth plastic versus metal rods), shape (curved plastic wall versus square metal wall), and odor (0.5% vanilla extract versus 33%

Simple Green)] for 3 minutes to measure baseline freezing. Acquisition of freezing responses is reported as percent freezing in the 60-second period following each of the 5 foot shocks, analyzed by two-way repeated measures ANOVA. 24-hour recall is reported as percent freezing in each context over the 3-min test period, analyzed by two-way repeated measures ANOVA.

Rotarod analysis

Mice were tested on rotarod (#47600; Ugo Basile) to evaluate motor deficits as described previously prior to BDNF delivery (6 weeks of age) and 4 weeks after the BDNF delivery started (11 weeks of age). Rotarod paradigm consisted of four trials per day over four days with acceleration from 5 to 40 rotations per minute (rpm) over minutes 0 to 5, followed by 40 rpm constant speed from 5 to 10 min. Latency to fall was recorded [27].

5-bromo-2'-deoxyuridine (BrdU) Administration

BrdU (Biolegend) was injected intraperitoneally following the final rotarod trial at a dosage of 100 mg/kg every 12 hours for a total of three doses. Mice were sacrificed 72 hours after the last injection as previously described [28].

Immunofluorescent (IF) staining

IF was performed on a minimum of six different floating 45-μm-thick brain slices from each mouse (six technical replicates per mouse per region or antibody of interest). Confocal images were acquired using a confocal microscope (Olympus FV1000) using a 20X oil objective. Z-stacks consisting of twenty non-overlapping 1-μm-thick slices were taken of each stained brain slice per brain region (i.e., six z-stacks per mouse, each taken from a different brain slice). The laser power and detector gain were standardized and fixed between mice within a surgery cohort, and all images for mice within a cohort were acquired in a single imaging session to allow for quantitative comparison.

We used primary antibodies against Purkinje cell marker calbindin (mouse, Sigma-Aldrich, C9848), neuronal marker neuronal nuclei (NeuN) (rabbit, Abcam, Ab104225), astrocytic marker glial fibrillary acidic protein (GFAP) (chicken, Millipore, AB5541), microglial marker ionized calcium binding adaptor molecule 1 (Iba1) (rabbit, WAKO, 019-19741), bromodeoxyuridine (BrdU) (rat, Bio-Rad, MCA2060), and vesicular glutamate transporter 2 (VGLUT2) (guinea pig, Millipore, AB2251-I) as previously described [29][30]. Quantitative analysis was performed using ImageJ (NIH) as described previously. To quantify relative intensity of staining for GFAP and calbindin we measured the average signal intensity in the region of interest and normalized it to that of the WT aCSF-treated mouse of that cohort. The density of neurons, astrocytes, microglia, and new neuronal cells was determined by normalizing the number of NeuN+, GFAP+, Iba1+, and BrdU+ cells respectively with the appropriate cellular morphology to the area of the region of interest. We determined GFAP+ and Iba1+ percent area by creating a mask of GFAP and Iba1 staining respectively and recording the fraction of the region of interest covered by staining. To quantify atrophy of the cerebellar molecular layer we took six measurements per image of the distance from the base of the Purkinje soma to the end of their dendrites, the average being the molecular layer width for that image. Recession of climbing fibers was quantified by normalizing the width of VGLUT2 staining to the width of the molecular layer. The width of hippocampal neuronal layers (CA2, and CA3) was measured by dividing the area of each neuronal layer by the length of that layer as previously described [16].

We also performed IF on 6-µm-thick slices from paraffin embedded cerebellum samples from human SCA1 patients and normal healthy controls provided to us by Dr. Arnulf H. Koeppen, Albany, NY (**Table 1**). Confocal images were acquired using a confocal microscope (Olympus FV1000) using a 40X oil objective. Z-stacks consisting of five 1-µm-thick slices were taken of each stained brain slice. The laser power and detector gain were standardized and fixed between samples. Human tissue was stained with BDNF (rabbit, Abcam). Percent area of staining for BDNF was quantified using the same method described for mouse confocal images.

To quantify BDNF+ puncta, we utilized the ImageJ analyze particles function that recorded the count and total area of particles between the size of 0.05 μm^2 and 5.0 μm^2 and a circularity between 0.5 and 1.0. We normalized particle counts and total particle area to the total area of the region of interest in order to calculate BDNF+ puncta density and BDNF+ puncta percent area, respectively. To quantify BDNF and GFAP overlap we used FIJI plug-in Coloc2 and macro to automatically quantify co-localization using Manders overlap coefficient (MOC). We used MOC due to its sensitivity to co-occurrence, the fraction of pixels with positive values for both channels, regardless of signal levels [31].

Table 1.

Region	Identifier	Sex	Age	CAG
Cblm	Control 1	M	70	
Cblm	Control 2	M	63	
Cblm	Control 3	F	63	
Cblm	Control 4	F	73	
Cblm	Control 5	F	69	
Cblm	SCA1	M	64	45
Cblm	SCA1	M	65	42
Cblm	SCA1	F	63	41
Cblm	SCA1	F	81	38
Cblm	SCA1	F	66	46

Enzyme-linked immunosorbent assay (ELISA)

Subcortical tissue was dissected on ice and the weight of the tissue for each mouse was measured, then frozen. Proteins were extracted from frozen tissue using Tris-Triton Lysis Buffer [150nM sodium chloride, 1.0% Triton X-100, 0.5% sodium deoxycholate, 0.1% SDS (sodium dodecyl sulfate), and 50mM Tris (pH 8.0)] as has been described previously [22]. Following lysate preparation, total BDNF was quantified in duplicates using the Total BDNF Quantikine ELISA kit (Biotechne-R&D Systems).

Reverse transcription and quantitative polymerase chain reaction (RT-qPCR)

Total RNA was extracted from dissected mouse cerebella, medulla, and hippocampus using TRIzol (Life Technologies), and RT-qPCR was performed as described previously [32]. We used primers listed in Table 2 as well as IDT Primetime primers for the following genes: *Aqp4,*

Gja1, Slc1a2, C3, Aif1, and Gapdh. Relative mRNA levels were calculated using 18S RNA as a control and wild-type mice as a reference using $2^{-\Delta\Delta-Ct}$ as previously described.

Table 2. Primer sequences

Gene name	**Forward Sequence (5'→3')**	**Reverse Sequence (5'→3')**
Calbindin1	AAG GCT TTT GAG TTA TAT GAT CAG	TTC TCA CAC AGA TCT TTC AGC
Gnarl3	TCA TGA AGC CGT GTG TGC	CAC GGA TGG GAG GTC ATC
Homer3	TGA AGA TGC TGT CAG AAG G	CTG TCC TGA AGC GCG AAG
Inpp5a	ATT CGG ACA CTT TGG AGA GC	CCT TTT CTT GAC CAT TTG CAC
Itpr	GAA GGC ATC TTT GGA AGT	ACC CTG AGG AAG GTT CTG
Rgs8	CTG TCA CAC AAA TCA GAC TCC TG	TGC TTC CGT GCA GAG TC
Kcnj10	*TCC GGG TTT AAG AGT CTT GG*	CTT AGC GAC CGA CGT CAT CT
Gfap	*AGA AAG GTT GAA TCG CTG CA*	CGG CGA TAG TCG TTA GCT TC
18s	*AGT CCC TGC CCT TTG TAC ACA*	CGA TCC GAG GGC CTC ACT A

Statistical analysis

Wherever possible, sample sizes were calculated using power analyses based on the standard deviations from our previous studies, significance level of 5%, and power of 90%. Statistical tests were performed with GraphPad Prism 7.0. Data was analyzed using two-way ANOVA (to assess the impact of genotype and treatment) followed by post-hoc two-tailed, unpaired Student's t-test (to test statistical significance of differences between groups of interest wherein only one variable was different (treatment or genotype), or one-way ANOVA followed by the Sidak's post-hoc test. Outliers were determined using GraphPad PRISM's Robust regression and Outlier removal (ROUT) with a Q=1% for non-biased selection.

Data availability

All the data from this study are available from the authors.

Results

Early stages of cerebellar pathology in Atxn1$^{154Q/2Q}$mice are characterized by the Purkinje cells pathology, mild reactive Bergmann gliosis and reduced microglial density in the cerebellar white matter

MRI brain scans of patients with SCA1 show a severe atrophy of the cerebellum while post-mortem brain investigations reveal pathology in the cerebellar cortex, white matter, deep cerebellar nuclei and the three cerebellar peduncles [6][13]. In addition, a recent longitudinal MRI study indicated significant cortical thinning of cerebellar cortex [33]. Cerebellar pathology, including thinning/atrophy of the molecular layer (ML), loss of Purkinje cell (PC) arbors, and recession of climbing fiber synapses on PCs is well described and used to quantify cerebellar degeneration in SCA1 mouse models [34][32]. Previous work has shown that at 12 weeks of age, *Atxn1$^{154Q/2Q}$* mice demonstrate robust and reproducible motor and cognitive deficits and early signs of PC dysfunction without neuronal loss [38]. During the regular sequencing we have found that the number of CAG repeats spontaneously expanded to 166 CAG in our colony. Thus we investigated how this larger CAG expansion affects neurons and glia in cerebellar cortex and deep cerebellar nuclei in 12 week old *Atxn1$^{154Q/2Q}$* mice.

To quantify PC pathology, we employed immunohistochemistry of cerebellar slices with antibodies specific for calbindin-1 (CALB1), a PC-specific marker (**Figure 1A**), and vesicular glutamate transporter 2 (VGLUT2), a marker of climbing fiber (CF) synapses on PC dendrites (**Supplementary Figure 1)** [35]. We found evidence of atrophy of PC dendritic arbors, as measured by the reduced thickness of the ML, and the reduced intensity of CALB1 staining in

the Purkinje cell layer (PCL) and ML in the primary fissure which is most commonly examined in mouse models of SCA1 (**Figures 1B-C**). Loss of CF synapses on PCs was measured as the ratio of width of VGLUT2 staining in the ML to the width of the ML (**Supplementary Figure 1)**[32]. We found a small but statistically significant reduction in the VGLUT2/ML ratio in the primary fissure lobules V and VI (**Figure 1D**), indicating synaptic loss. We also examined molecular PC alterations examining gene expression changes by RT-qPCR of the selected Magenta Module genes including *Calb1*, *Inpp51*, *Garnl3*, *ITPR*, *Homer 3*, and *Rgs8.* The Magenta Module was identified by RNA-sequencing as a hub of genes whose increasingly reduced expression correlates with the progression of PC pathology in transgenic *ATXN1[82Q]* mice and in knock-in *Atxn1*$^{154Q/2Q}$ mice [36]. We performed RT-qPCR on whole-cerebellum RNA and found a significant reduction- to about 50% of control- in the expression of *Calb1*, *Inpp51*, *Garnl3*, *ITPR*, *Homer 3*, and *Rgs8* at 12 weeks in cerebella of *Atxn1*$^{154Q/2Q}$ mice (**Supplementary Figure 2**). Thus we can detect PC pathology, including dendritic atrophy, loss of synapses and altered gene expression in 12 week old *Atxn1*$^{154Q/2Q}$ mice.

PCs are the main output from the cerebellar cortex and project to cerebellar nuclei (CN) that drive the main output from the cerebellum [37]. CN pathology is described in end-stage SCA1 patients but little is known about CN pathology in mouse models of SCA1 [13]. To investigate pathology of the CN, we quantified neural (NeuN+) cell density in the interposed and fastigial cerebellar nuclei. We found no significant difference in the number of NeuN+ cells per area between WT and *Atxn1*$^{154Q/2Q}$ mice in either cerebellar nucleus (**Supplementary Figure 3**).

Bergmann glia (BG) are a subtype of cerebellar astrocytes that have a very intimate structural and functional relationship with PCs [38][39]. To investigate changes in BG we quantified an increase in area occupied by glial fibrillary acidic protein (GFAP) (percentage of area that is GFAP+), a morphological characteristic of hypertrophy in reactive astrocytes and an

increase in GFAP immunoreactivity, often used as measure of astrogliosis [40][41]. We detected a significant increase in GFAP+ percent area in the primary fissure (**Figure 1E**), indicating reactive hypertrophy. but found no significant increase in the intensity of GFAP staining [42] (**Supplementary Figure 4**). BG are critical for the function of PCs in part because they remove excess extracellular neurotransmitters (i.e. glutamate via glutamate transporters GLAST encoded by *Slc1a3* gene) and maintain homeostatic extracellular levels of ions (e.g. potassium via potassium channel Kir4.1 encoded by *Kcnj10*) and water (through the expression of Aquaporin-4, encoded by *Aqp4*)[43][44][45][46]. To evaluate the functional state of reactive BG in the cerebella of *Atxn1*$^{154Q/2Q}$ mice, we quantified the expression of these critical BG genes using RT-qPCR of whole cerebellar extracts. We have found a slight increase in the expression of *Aqp4*, *Gja1*, *Kcnj10*, *Slc1a3* and *C3* but none were statistically significant due to the large variability of expression in *Atxn1*$^{154Q/2Q}$ mice (**Supplementary Figure 5**). Our previous studies indicated that reactive cerebellar astrocytes show pre-symptomatic increase in the expression of neuroprotective genes followed by a decrease in the expression of neuroprotective genes with disease progression [47]. It is possible that increased variability in cerebellar astrocytic gene expression indicates that cerebellar reactive astrocytes are undergoing shift in their phenotype at this disease stage

We have previously shown that microglia are reactivate in SCA1 cerebellar cortex and contribute to SCA1 pathogenesis [27][48]. To test if this is altered with CAG expansion, we applied IHC staining for the microglial marker ionized calcium binding adaptor protein (Iba1) encoded by *Aif1* and quantified microglial density and the percent area covered by microglial Iba1+ processes (**Figure 1F, Supplementary Figure 6A**). We found no significant change in microglia density or the Iba1+ percent area in the molecular nor in the granule cell layer of *Atxn1*$^{154Q/2Q}$ mice (**Supplementary Figure 6B**). However, there was a significant reduction in microglia density and the Iba1+ percent area in the cerebellar white matter of *Atxn1*$^{154Q/2Q}$ mice

compared to WT controls (**Figure 1G**). Consistent with these results, expression of Iba1-encoding gene *Aif1* in the whole cerebellum was significantly reduced (**Figure 1H**). These findings indicate that at this early disease stage in SCA1 knock-in mice expressing mutant ATXN1 with 166 glutamine repeats there is detectable PC pathology, hypertrophy of BG in the cerebellar cortex, and reduced microglial density in the cerebellar white matter.

Early astrocytic pathology in the SCA1 medulla oblongata precedes neuronal loss and is characterized by reduction in astrocytic cell density and reduced expression of astrocytic homeostatic genes in Atxn1$^{154Q/2Q}$ mice

As mutant Ataxin-1 is widely expressed [49][28][16], we sought to investigate neuronal and glial pathology in brain regions beyond the cerebellum, in particular the medulla oblongata, hippocampus, and motor cortex. These regions have presumptive roles in premature lethality as well as motor and cognitive dysfunction in SCA1. For instance, aspiration pneumonia is one of the leading causes of death in patients with SCA1 [8]. Neuronal degeneration and gliosis have been documented in the medulla oblongata of patients with SCA1 and are thought to contribute to the loss of ability to protect airways and, subsequently, aspiration pneumonia and death [8][50].

Thus to increase our understanding of neuronal and glial pathology in the medulla oblongata of *Atxn1*$^{154Q/2Q}$ mice, we used NeuN, GFAP and Iba1 IHC to quantify neuronal density and gliosis in the medial vestibular nucleus (MVN), lateral reticular nucleus (LRN), and inferior olivary nucleus (ION). We chose these nuclei because of their roles in balance, respiration, and cerebellar learning, all important phenotypes of SCA1 [41]. Moreover, postmortem analysis of patient samples has previously determined degeneration in each of these nuclei with severe loss of volume in the ION and LRN [6].

At this early disease stage in *Atxn1*$^{154Q/2Q}$ mice we did not detect a significant difference in the neuronal (NeuN+ cells) density in any of these regions (**Figures 2A-D**). Astrocyte reactivity was

quantified by measuring GFAP staining intensity, morphological changes, and cell density in the inferior olive of WT and *Atxn1*$^{154Q/2Q}$ mice. We specifically focused on the inferior olive due to the clarity and high-quality of astrocyte staining relative to other medullar nuclei (**Figure 2E**). Interestingly, we found that in the inferior olive of *Atxn1*$^{154Q/2Q}$ mice the intensity of GFAP staining was significantly reduced (by about 40%). Likewise, there was a significant reduction in the density of astrocytes in 12-week-old *Atxn1*$^{154Q/2Q}$ mice (**Figures 2F-G**). We also found a significant reduction in the expression of astrocyte specific genes *Gfap, Aqp4*, *Gja1, Slc1a1, Kcnj10, and C3* in medulla of *Atxn1*$^{154Q/2Q}$ mice (**Figure 2H**). It is unclear to what extent these changes are caused by astrocyte loss and/or decreased expression of these genes in the surviving astrocytes. Given the importance of these homeostatic astrocytic genes for neuronal function, our results may indicate a novel mechanism by which astrocytes contribute to neuronal dysfunction in the medulla of *Atxn1*$^{154Q/2Q}$ mice.

Finally, we found a slight but significant increase in microglial density in the MVN and ION of 12-week-old *Atxn1*$^{154Q/2Q}$ mice **(Figure 2I**). There was no change in Iba1 percent area nor in the *Aif1* mRNA expression (**Supplementary Figure 7**).

Together, these results indicate that, early in SCA1 disease astrocyte density and astrocyte-specific gene expression are reduced in the medulla of 12-week-old *Atxn1*$^{154Q/2Q}$ mice. This occurs before any measurable loss of neurons within the assessed medullar nuclei but is concurrent with an increase in microglial density. Remarkably, these effects are distinct from the trends seen in the cerebellum which include mild cerebellar astrocytes reactivity and loss of microglia in cerebellar white matter. Together, these results suggest that SCA1 astrocytes and microglia in the cerebellum and medulla undergo region-specific alterations.

Adult hippocampal neurogenesis and the expression of homeostatic genes in the hippocampal astrocytes are decreased in Atxn1$^{154Q/2Q}$ *mice*

While several studies have demonstrated mild cognitive deficits, including visuospatial and memory dysfunctions in some patients with SCA1 [51][14][52][53][54][55][56], very few studies examined hippocampal pathology in patients. A recent volumetric MRI study demonstrated a slight but not statistically significant decrease in hippocampal volume in patients with SCA1 [11]. In addition, previous studies have described impaired performance of *Atxn1*$^{154Q/2Q}$ mice in cognitive tests including the Morris Water Maze, Barnes maze, and contextual fear conditioning at 7-12 weeks of age [14][15]. Neuronal dysfunction and neuronal loss in the hippocampus have been described at 24 weeks [14][16], and hippocampal neurogenesis was reduced at 12 weeks in *Atxn1*$^{154Q/2Q}$ mice [17].

To confirm this previous finding in our expanded mouse line, we quantified hippocampal neurogenesis by measuring proliferation in the dentate gyrus. We injected 12–week-old WT and *Atxn1*$^{154Q/2Q}$ mice with the DNA-integrating marker of proliferation bromodeoxyuridine (BrdU). We found that *Atxn1*$^{154Q/2Q}$ mice had significantly fewer proliferating (BrdU+) cells per area relative to WT mice, confirming that expanded *Atxn1*$^{154Q/2Q}$ mice have reduced hippocampal neurogenesis at 12 weeks (**Figures 3A-B**).

As hippocampal neurogenesis can be affected by non-cell autonomous effects, we next examined neuronal and glial pathology in the hippocampus of 12-week-old *Atxn1*$^{154Q/2Q}$ mice. Though these mice have been shown to exhibit significant thinning at later time points [25], we did not find significant thinning of CA2 or CA3 in 12-week- old *Atxn1*$^{154Q/2Q}$ mice (**Supplementary Figure 8A**).

RT-qPCR analysis demonstrated significant downregulation of astrocyte-specific genes *Gfap, Kcnj10*, *Aqp4, Gja1, Slc1a2 and C3* in the hippocampus *Atxn1*$^{154Q/2Q}$ mice (**Figure 3C**). We found increases in intensity of GFAP staining, astrocyte cell density and in GFAP+ percent area in the dentate gyrus of *Atxn1*$^{154Q/2Q}$ mice relative to WT littermate controls. However, this failed to reach statistical significance (**Supplementary Figure 8B**). Thus, the relative expression of hippocampal astrocyte-specific genes followed a similar pattern as was seen in the medulla. Yet

in contrast, where we see a loss of GFAP intensity in SCA1 medulla, we have found a trending increase in the GFAP intensity in the hippocampus.

Furthermore, while changes in the number of microglia were seen in the cerebellum (decrease in white matter) and medulla (slight increase in MVN and ION), we found no significant change in Iba1 density or Iba1+ percent area in the hippocampus (**Supplementary Figure 8C**).

Microglia density and expression of astrocyte homeostatic genes are increased in the cortex of Atxn1$^{154Q/2Q}$ mice

Previous brain-wide investigation demonstrated neuronal loss in the primary motor cortex of SCA1 patients [6]. Because of the weak GFAP expression in the upper cortical layers, to assess pathology within motor cortex of *Atxn1*$^{154Q/2Q}$ mice we quantified neuronal and glial density, GFAP intensity and GFAP and Iba1 percentage area in the layer 6 of the motor cortex and the underlying corpus callosum (**Figure 4A**). We found no statistical difference in the density of neuronal (NeuN+) cells in the layer 6, indicating no detectable neuronal loss in the motor cortex of *Atxn1*$^{154Q/2Q}$ mice at 12 weeks of age (**Figure 4B**). GFAP intensity, cell density, and GFAP % area were slightly but not significantly increased the corpus callosum and not altered in layer 6 in *Atxn1*$^{154Q/2Q}$ mice compared to WT littermate controls (**Figures 4C-D**). There was a significant increase in the density of Iba1+ microglia and Iba1 % area both in the layer 6 and in the corpus callosum, indicative of cortical and white-matter microgliosis early in disease progression in *Atxn1*$^{154Q/2Q}$ mice (**Figures 4 E-F**).

Examination of glial gene expression in the bulk cortical tissue extracts showed an increase in the expression of the microglial gene *Aif1* consistent with the increased microglia density (**Figure 4G**). We have also found a significant increase in the expression of *Gfap* and the astrocytic homeostatic genes *Gja1*, *Kcnj10* and *Aqp4* (**Figure 4E**). This pattern of astrocytic

gene expression changes may indicate a compensatory state of cortical astrocytes that may be induced by or in response to microglial reactivity in *Atxn1*$^{154Q/2Q}$ mice. These changes in cortical astrocytic gene expression are distinct to those we have found in the cerebellum, hippocampus and medulla.

BDNF expression is reduced in cerebellar Bergman glia in patients with SCA1

We previously demonstrated that BDNF expression is altered in the cerebellum of the Purkinje cell-specific *Pcp2-ATXN1[82Q]* transgenic mouse model of SCA1. Specifically, we found an increase in cerebellar BDNF expression early in SCA1, followed by decreased BDNF expression as the disease progressed [22]. Furthermore, our previous results indicate that astrocytic NF-κB signaling contributes to altered BDNF expression in the cerebellum of *Pcp2-ATXN1[82Q]* mice [22]. Together, this implicates reduced BDNF expression as one mechanism by which cerebellar astrocytes may modulate the SCA1 pathogenesis. Importantly, our preclinical studies in *Pcp2-ATXN1[82Q]* mice have demonstrated that delivering BDNF early in disease and prior to motor symptom onset protects against the progression of cerebellar SCA1 pathology [6].

To further determine the clinical relevance of these findings, we investigated whether BDNF is altered in cerebellar astrocytes from patients with SCA1. Cerebellar slices of five patients with SCA1 and five sex- and age-matched healthy controls (**Table 1**) were co-stained with GFAP to label astrocytes and with BDNF to quantify its expression in cerebellar Bergmann glia (**Figures 5A C-D**). Using confocal microscopy, we found a decrease in the width of the molecular layer, indicative of PC atrophy in SCA1 patients as expected (**Figure 5B**). Our results also show increased GFAP intensity and GFAP % area in the molecular layer in patients with SCA1 compared to age-matched unaffected individuals, indicative of reactive Bergmann gliosis (**Figure 5B**). Importantly, the density and the area occupied by the BDNF labeled puncta were

significantly reduced in the ML of patients with SCA1. We also found a reduced co-localization of BDNF in GFAP stained BG compartments, indicating that reactive BG have decreased abundance of BDNF [57](**Figure 5E**). These results suggest that reduced expression of BDNF in the cerebellum is a feature of SCA1 in patients and is, at least in part, contributed to by decreased BDNF expression in BG.

Heterogenous changes in BDNF expression across brain regions in Atxn1$^{154Q/2Q}$ mice

Reduced BDNF in postmortem cerebella of SCA1 patients further supports our previous findings of the therapeutic potential and clinical relevance of BDNF. In the transgenic *Pcp2-ATXN1[82Q]* mouse model, mutant ATXN1 protein is expressed only in cerebellar PCs [61], thus pathology is limited to the cerebellum [58]. However, endogenous ATXN1 is widely expressed in the brain including the brainstem, cortex and hippocampus all of which are affected in SCA1 patients and *Atxn1$^{154Q/2Q}$* mice. As our results indicate that there are differences in the SCA1 astrocytic and microglial pathology in these regions, we next investigated how is expression of BDNF changed in the cerebellum, medulla, hippocampus and cortex of *Atxn1$^{154Q/2Q}$* mice. Supporting our previous findings in the *Pcp2-ATXN1[82Q]* mice, we found reduced *Bdnf* mRNA expression in the cerebellum of *Atxn1$^{154Q/2Q}$* mice. We also found a significant *Bdnf* reduction in the hippocampus, whereas the cortex and medulla exhibited a significant increase in the *Bdnf* expression in 12-week-old *Atxn1$^{154Q/2Q}$* mice (**Figure 6**). These regional differences in the BDNF expression in early SCA1 could reflect asynchronous progression of disease in different brain regions and indicate that therapeutic benefits of BDNF may also be region-specific.

BDNF rescues motor and aspects of cognitive deficits in symptomatic Atxn1$^{154Q/2Q}$ mice.

To test the therapeutic effects of BDNF on different SCA1 phenotypes and brain regions we initiated BDNF treatment at 7 weeks of age [23]. Prior to surgical implantation of ALZET pumps (delivering BDNF or aCSF vehicle), *Atxn1*$^{154Q/2Q}$ mice and WT littermate controls were subjected to motor and cognitive testing as well as body weight analysis. This was done both to determine whether expanded repeat *Atxn1*$^{154Q/2Q}$ mice exhibited disease phenotypes at 7 weeks. As early as 6 weeks of age, *Atxn1*$^{154Q/2Q}$ mice showed a significant deficit in motor coordination as seen by a shorter latency to fall on the rotarod assay (**Supplementary Figure 9A**). *Atxn1*$^{154Q/2Q}$ mice also exhibited cognitive impairment evident by their significantly reduced time spent freezing in a contextual fear conditioning assay at this time point (**Supplementary Figure 9B**). Body weight comparisons between genotypes also showed that *Atxn1*$^{154Q/2Q}$ mice were significantly underweight relative to WT controls (**Supplementary Figure 9C**). Notably, there was no significant difference among *Atxn1*$^{154Q/2Q}$ or WT mice randomly assigned to aCSF or BDNF treatment groups. Mice then underwent surgery in which a cannula was implanted into the right lateral ventricle and an ALZET pump was placed subcutaneously to deliver BDNF or aCSF for four weeks. BDNF delivery was confirmed using ELISA at the end of the experiment at 13 weeks of age (**Supplementary Figure 10**). Out of 42 mice that underwent surgery five died unexpectedly. Four of those mice received BDNF delivery and three of these five mice were *Atxn1*$^{154Q/2Q}$ mice**.**

Motor deficits were examined via rotarod after four weeks of BDNF delivery. BDNF significantly improved the rotarod performance of *Atxn1*$^{154Q/2Q}$ mice confirming beneficial effect of BDNF on motor deficits in this SCA1 model (**Figure 7A**). Intriguingly, BDNF also enhanced performance of WT mice.

Study mice were also tested on Barnes maze and re-tested on contextual fear conditioning 3 weeks after pumps were implanted. *Atxn1*$^{154Q/2Q}$;BDNF mice had a reduced the latency to enter the escape hole during the training phase of Barnes maze compared to *Atxn1*$^{154Q/2Q}$;aCSF controls (**Figure 7B**), suggesting that BDNF has a beneficial effect on learning (i.e. enhances

the ability of *Atxn1*$^{154Q/2Q}$ mice to effectively find the escape hole). To further examine how BDNF affects learning, we used the automated Barnes maze unbiased strategy analysis tool (BUNS)[26]. Mice can solve the Barnes maze using spatial strategies (direct, corrected, long correction and focused search indicated by black to red colors in Figure 7), non-spatial search strategy (serial, going around the maze until they find escape hole, indicated by yellow color), or by randomly exploring the maze (using no strategy at all, indicated by white color) (**Supplementary Figure 11**). We have previously shown that *Atxn1*$^{154Q/2Q}$ mice preferentially use random and serial strategies instead of spatial strategies to find the escape hole [15]. Our expanded *Atxn1*$^{154Q/2Q}$ mice also used less spatial strategies (6.25% compared to 26% spatial strategy use by wild-type mice), confirming our previously described cognitive deficits in developing higher-level problem-solving strategies in *SCA1* models [17] (**Figure 7C**). Importantly, we found that BDNF significantly improved strategy development in *Atxn1*$^{154Q\ /2Q}$ mice (from 6.25% use of spatial search strategies, including direct, corrected, long corrected and focused search, in *Atxn1*^{154Q};aCSF mice to 18% use of spatial strategies in *Atxn1*^{154Q} ;BDNF treated mice, **Figure 7C**). Each strategy is assigned cognitive score, and linear regression analysis of the rate of cognitive score change per training day also demonstrated that BDNF significantly improved strategy development in *Atxn1*$^{154Q/2Q}$ mice **(Supplementary Figure 12C**). These results suggest that BDNF has a remarkable effect on the strategy development in *Atxn1*$^{154Q/2Q}$ mice.

As we previously demonstrated, control (aCSF treated) WT mice exhibited significantly more freezing than *Atxn1*^{154Q} mice on the repeated fear conditioning [17], while there was no significant difference between BDN treated WT and *Atxn1*^{154Q} mice (**Supplementary Figure 12C**). Despite previous studies linking BDNF and body weight [59], BDNF had no effect on the failure to gain weight phenotype in *Atxn1*$^{154Q/2Q}$ mice (**Supplementary Figure 12D**).

BDNF ameliorates hippocampal neurogenesis and hippocampal astrocyte gene expression deficits in Atxn1$^{154Q/2Q}$mice

BDNF has been previously shown to regulate hippocampal neurogenesis [60][61][62][63][64], and *Atxn1*$^{154Q/2Q}$ mice exhibit both reduced hippocampal neurogenesis and reduced BDNF expression in the hippocampus. Therefore, we next investigated whether delivery of exogenous BDNF ameliorated SCA1 deficits in hippocampal neurogenesis. Using BrdU incorporation, we found an increased number of proliferating (BrdU labeled) cells in the dentate gyrus of BDNF-treated *Atxn1*$^{154Q/2Q}$ mice to levels similar to that of aCSF-treated WT mice (**Figures 8A-B**). These results indicate that BDNF rescues hippocampal neurogenesis deficits in *Atxn1*$^{154Q/2Q}$ mice. Notably, as previously indicated, BDNF also caused a trending increase in hippocampal neurogenesis in WT mice.

BDNF also had a significant effect on the neuronal layer thickness in CA3 area in wild-type and *Atxn1*$^{154Q/2Q}$ mice (effect of treatment by two way ANOVA $F(1,14)=6.4$, $p = 0.02$) but not effect on CA2 area (**Figure 8C**).

BDNF receptors are expressed on astrocytes and as such exogenous BDNF can also directly affect astrocytes [65][66]. In the hippocampus, BDNF treatment increased the expression of astrocyte homeostatic genes *Aqp4, Gja1, C3, Gfap, Kcnj10 and Slc1a3* in *Atxn1*$^{154Q/2Q}$ mice as well as in WT mice (**Figure 8D**). Notably, GFAP protein levels were also significantly increased in the hippocampus of BDNF-treated WT mice, though this did not extend to *Atxn1*$^{154Q/2Q}$ mice (**Figure 8E**).

BDNF caused significant increase in microglial density in two different regions of hippocampus that we examined, the dentate gyrus granule cell layer and hilus of wild-type mice, and a trend towards increase in *Atxn1*$^{154Q/2Q}$ mice (**Supplementary Figures 13A-B**). BDNF showed trending increase in *Aif1* mRNA in the hippocampus of WT mice (**Supplementary Figure 13C**).

BDNF also had positive effect in other brain regions affected in SCA1. In the cerebellum, BDNF had slight beneficial effects on PCs, astrocytes and microglia. At 12 weeks of age, the predominant neuronal pathology is a thinning of the ML of the cerebellar cortex, indicating PC dendritic atrophy (**Figure 1, Supplementary Figure 14A**). BDNF application slightly ameliorated ML thickness *Atxn1*$^{154Q/2Q}$ mice (from 168 .9± 5.4 µm in aCSF to 184.1 ± 10.1 µm in BDNF treated *Atxn1*$^{154Q/2Q}$ mice) however this did not reach statistical significance (**Supplementary Figure 14C**). GFAP % area in cerebellar cortex and microglial density in white matter were not significantly altered with BDNF treatment (**Supplementary Figures 14A-E**). BDNF increased expression of PC genes associated with SCA1 progression *Calbindin, Inpp51, ITPR, Homer3, and Rgs8* (Magenta Module genes) in wild-type mice (reaching statistical significance only for *Inpp51*), and to a lesser degree in *Atxn1*$^{154Q/2Q}$ mice (none reached statistical significance) (**Supplementary Figure 14F**)**.** BDNF significantly increased expression of cerebellar astrocytic gene *Gfap* and microglial gene *Aif1* in wild-type mice and to a lesser extent in *Atxn1*$^{154Q/2Q}$ mice, as well as caused a trending increase in the expression of *Kcnj10* and *Gja1* in wild-type mice (**Supplementary Figure 14G-H**).

In the medulla, BDNF had a significant beneficial effect on neurons, trending beneficial effect on microglia, and a mixed effect on astrocytes. BDNF significantly increased neuronal density within the lateral reticular nucleus in *Atxn1*$^{154Q/2Q}$;BDNF mice (**Supplementary Figures 15 A, D).** interestingly, BDNF caused a significant decrease in astrocyte density, GFAP intensity and expression of *Aqp4* and *Gfap* in the medulla of wild-type mice. On the other hand, 2-way ANOVA showed significant effect of BDNF on increasing the expression of *Kcnj10* ($F(1,14) = 6.41$, $P = 0.02$) (**Supplementary Figures 15 B, E, G**). BDNF significantly reduced microglial density in lateral reticular nucleus of wild-type mice, and caused a trending decrease in microglial density in the medial vestibular nucleus of *Atxn1*$^{154Q/2Q}$ mice (**Supplementary Figures 15 C, F, G**).

In the motor cortex BDNF significantly affected microglia and astrocytes but had no effect on neuronal density (**Supplementary Figure 16 A-B**). In wild-type mice, BDNF increased astrocytic expression of *Gfap* and *Aif1*, as well as the Iba1 % area in corpus callosum, while the opposite effects, a trending decrease in astrocytic expression of *Gfap* and *Aif1*, and in Iba1 % area in corpus callosum, were seen in the *Atxn1*$^{154Q/2Q}$ mice (**Supplementary Figure 16 C-F**). BDNF caused significant increase in *C3* expression and a trending increase in GFAP intensity, GFAP % area, GFAP cell density in layer 6 in both wild-type and *Atxn1*$^{154Q/2Q}$ mice.

In summary, while BDNF had some protective effects on neurons, astrocytes and microglia in all examined brain regions, it was most beneficial in the hippocampus, where it rescued expression of astrocyte homeostatic gene expression and adult hippocampal neurogenesis.

Discussion

Here, we report on the spectrum of altered BDNF expression, reactive astrocyte and microglia phenotypes, across several clinically relevant brain regions of *Atxn1*$^{154Q/2Q}$ mice in the early stages of disease progression. Importantly, we demonstrated that BDNF is decreased in the cerebellar astrocytes in patients with SCA1 as we have seen in our mouse models. Finally, we demonstrated the therapeutic effects of BDNF on several SCA1 phenotypes, including motor and cognitive deficits, and SCA1 pathology of neurons, astrocytes and microglia in hippocampus, cerebellum, medulla, and motor cortex.

Recent studies indicated heterogeneity of glial cells across brain regions [67] and across different disease conditions [68][40]. Our results indicate that early stages of disease in our expanded *Atxn1*$^{154Q/2Q}$ mice are characterized by morphological and molecular changes only in cerebellar Purkinje cells and pronounced heterogenous changes in astrocytes and microglia across multiple brain regions. This spectrum of reactive glial phenotypes may reflect asynchronous progression of disease in different brain regions as well as brain-region-specific

astrocytic, neuronal and microglial dysfunctions. Given that these changes precede neuronal loss, it is crucial to examine glial heterogeneity as means to distinguish protective versus deleterious astrocytic phenotypes and identify opportunities for early therapeutic intervention. For this reason, we focused here of the astrocytic neuroprotective genes *Slc1a2*, *Kcnj10*, *Gja1*, and *Aqp4*, and found that their expression was reduced in the medulla and hippocampus, but was increased in the cortex of *Atxn1*$^{154Q/2Q}$ mice at 12 weeks of age and before notable neuronal loss [69]. *Kcnj10* encodes a potassium rectifier, Kir4.1, that is involved in maintaining potassium homeostasis [70] and has been implicated in several diseases, including Huntington's disease, ALS, and depression [71][70][72]. Connexin 43 (*Gja1)* is involved in astrocyte communication [21]. Aquaporin (*Aqp4)*, is critical for both interstitial fluid drainage in the glymphatic system and water homeostasis [73]. Astrocytic *Slc1a* (2 and 3) genes encode glutamate transporters that are responsible for removing glutamate from synaptic space. As such, these astrocytic genes are critical for neuronal function, and have been implicated in the pathogenesis of several neurodegenerative diseases [74][75]. We propose that reduced expression of astrocyte neuro-supportive genes contributes to neuronal dysfunction and SCA1 pathogenesis in the hippocampus and medulla. Conversely, increased expression of these neurosupportive astrocyte genes in the cortex may indicate compensatory roles of astrocytes that delays neuronal dysfunction in the SCA1 cortex.

We found no evidence of increased GFAP expression, a hallmark of reactive astrogliosis, in the medulla. Likewise, we found only trending indication of GFAP defined gliosis in the hippocampus. Thus, our results may indicate that increased GFAP expression may not directly correlate to changes in astrocyte homeostatic gene expression in disease conditions. This is consistent with a previous study which demonstrated that reduced expression of the astrocyte homeostatic gene *Kcnj10* in the striatum of Huntington's mice is not dependent on astrogliosis as defined as increased GFAP expression [70].

Our work also revealed an unexpected loss of astrocytes in the medulla of 12-week-old *Atxn1*$^{154Q/2Q}$ mice. Although surprising as it preceded neuronal loss, this is consistent with previous work that showed lower levels of *myo*-inositol (Ins), an astrocytic marker, in the brainstem of 18- and 28-week-old *Atxn1*$^{154Q/2Q}$ mice [5]. Moreover, treatment with *Atxn1* targeting antisense oligonucleotides (ASO), which are also taken up by astrocytes [76], was shown to rescue lower Ins levels in the brainstem and prolong the survival of *Atxn1*$^{154Q/2Q}$ mice [5]. Based on these results we propose that *ATXN1 e*xpression in the astrocytes reduces expression of homeostatic genes and decreases astrocyte viability in cell autonomous manner, contributing and possibly initiating medullar dysfunction and eventual premature lethality. However, while neuronal numbers were not altered in medulla of 12-week-old *Atxn1*$^{154Q/2Q}$ mice, we cannot exclude neuronal dysfunction. Future studies using conditional SCA1 mice to selectively delete expression of mutant ATXN1 in astrocytes will provide insight into the cell autonomous effect of mutant ATXN1 on astrocyte pathology in the medulla and other brain regions in SCA1.

Building on our previous work showing BDNF therapeutic promise in cerebellum specific SCA1 mice, here we demonstrate that BDNF is decreased in Bergmann glia processes in the cerebellum of patients with SCA1 compared to unaffected age-and sex- matched controls. In addition, we found increased GFAP expression and GFAP percent area together indicating that reactive astrogliosis of Bergman glia and reduced BDNF are features of SCA1 in patients. Moreover, we found a spectrum of brain region-specific changes in BDNF expression in the *Atxn1*$^{154Q/2Q}$ mice that was predictive of BDNF's therapeutic effectiveness across different brain regions and SCA1 phenotypes. The cerebellum and hippocampus showed reduced BDNF expression while BDNF expression was increased in the medulla and cortex of 12-week-old *Atxn1*$^{154Q/2Q}$ mice. We propose that heterogeneity of BDNF expression changes may be indicative of regional differences in the SCA1 pathology in terms of the timing of cellular

pathology but also of differences in physiological levels of BDNF expression and cells that produce it in different regions. Regardless, these results confirm our previous findings from transgenic mouse model of SCA1 and lend further support to the translational potential of BDNF delivery in SCA1.

Our previous studies demonstrated that exogenous BDNF delivery during the early disease stage protected against cerebellar pathology and motor deficits in the transgenic *ATXN1[82Q]* model of SCA1 mice and was more beneficial than treatment at later stages of disease [22][23]. Here, we extended these findings to demonstrate that exogenous BDNF significantly ameliorated several SCA1 phenotypes in *Atxn1*$^{154Q/2Q}$ mice. BDNF ameliorated motor deficits and improved learning and strategy development. This was accompanied by a rescue of hippocampal neurogenesis and astrocyte homeostatic gene expression in the hippocampus of BDNF treated *Atxn1*$^{154Q/2Q}$ mice.

These results indicate therapeutic potential of BDNF in SCA1. It is important to note that BDNF did not rescue all SCA1 phenotypes and had a less of a significant effect on the pathology in the medulla, cortex and cerebellum of *Atxn1*$^{154Q/2Q}$ mice with many trending ameliorations. Considering that at this early stage of SCA1 progression in *Atxn1*$^{154Q/2Q}$ mice BDNF is increased in medulla and cortex, it is not surprising that BDNF had lesser effect on pathology in these regions compared to hippocampus, where BDNF is decreased. In the cerebellum, BDNF showed trending rescue of PC atrophy and gene expression, astrocytic and microglial gene expression changes.

The region specific effectiveness on BDNF may also indicate variability in the potential for reversibility of pathological changes in different brain regions. For instance, reduced astrocyte density in medulla may be irreversible. Astrocyte and microglia heterogeneity across brain regions may also contribute to the brain region specific effect of BDNF. This is supported by the different effects of BDNF that we observed on astrocytes and microglia from different brain

regions in the WT mice. It is important to note that we cannot distinguish whether BDNF directly or indirectly affects astrocytes, neurons or microglia or if similar effects will be seen in human cellular counterparts. Future studies using human neurons, astrocytes and microglia derived from induced pluripotent cells (iPSCs) donated by patients with SCA1 will allow us to interrogate direct effects of BDNF on each human cell type [77].

BDNF plays a key role in a healthy brain function and loss of BDNF can contribute to pathology in neurodegenerative diseases and depression [78]. In addition to our findings in SCA1 patients and model mice, decreased expression of BDNF in patients and in mouse models has been described in other polyQ neurodegenerative diseases such as Huntington's disease (HD)[4][5] and SCA6 [6] [7]. Decreased BDNF has also been shown to correlate with behavioral impairments in aging, Alzheimer's disease (AD), and Parkinson's disease (PD) [8][9][10][11][12]. Despite differences in brain region and neuronal vulnerability in these diseases, BDNF treatment has been shown to be beneficial [22][23][13][14][15][16][17], indicating that BDNF has a great therapeutic potential with a broad disease target [79][80][81][82][83]. Our study further supports these findings adding SCA1 to the list of disorders for which BDNF is of relevance. We also build up on these studies indicating that BDNF may be altered in brain region specific manner in disease as well as that some of the beneficial effects of BDNF may be due to its effect on astrocytes and microglia

Acknowledgements:

We are very grateful to Dr. Arnulf H. Koeppen, Albany, NY for sharing cerebellar and medullar samples from patients with SCA1 and for the thoughtful feedback

We acknowledge all the members of Orr and Cvetanovic laboratories for thoughtful discussions and feedback on the study. Work in this study was aided by the Mouse Behavioral Core and Histology and IHC Laboratory at the University of Minnesota.

Funding:

This work was supported by National Institute of Health NINDS awards (R01 NS197387 and R01 NS109077 to M.C.)

Author Contributions:

M.C. conceptualized the study. J-G.R., C.S., K.H., A.S., and S.G. performed experiments. J-G.R., M.C., F.G., and C.S. analyzed data. M.C., and J-G.R., wrote the manuscript with input from H.T.O., A. K., C.S., K.H., A.S., and S.G.

Conflicts of Interest:

The authors report no conflicts of interest.

Figure legends

Figure 1.Early cerebellar pathogenesis is characterized by neuronal and glial changes in *Atxn1*$^{154Q/2Q}$ mice. Cerebellar sections from 12 weeks old *Atxn1*$^{154Q/2Q}$ and wild-type littermate controls (N = 3-5) were stained for calbindin (A), VGLUT2, GFAP and Iba1 (F). Confocal images at primary fissure lobules V/VI were used to measure molecular layer width (B), calbindin expression (C), length of VGLUT2 synapses on Purkinje cell dendrites as a measure of climbing fiber extensions on PCs (D), GFAP percent area (E) and density of microglia (G). H. Quantitative RT-PCR showing expression of microglial marker Aif1. Data is presented as mean ± SEM with average values for each mouse represented by a dot. * $p<0.05$ Students t-test.

Figure 2. Early SCA1 pathology in medulla of *Atxn1*$^{154Q/2Q}$ mice is characterized by astrocytic loss. Brain sections from 12- week- old *Atxn1*$^{154Q/2Q}$ and wild-type littermate controls (N = 3-5) were stained for NeuN (A) and GFAP (E). Confocal images from each mouse were used to quantify neuronal (B-D), GFAP expression (F), density of astrocytes (G), and microglia

(I). H. mRNA was extracted from the medulla dissected from 12 weeks old *Atxn1*$^{154Q/2Q}$ and wild-type littermate controls (N = 4-6) and RTqPCR was used to evaluate expression of astrocyte specific genes. Data is presented as mean± SEM with average values for each mouse represented by a dot. * p<0.05 Students t-test.

Figure 3. Early SCA1 pathology in the hippocampus of *Atxn1*$^{154Q/2Q}$ mice is characterized by reduced hippocampal neurogenesis and decreased astrocytic gene expression. A-B. Mice were injected with BrdU to label proliferating cells in the hippocampal dentate gyrus. Slices were stained with BrdU antibody and confocal images were used to quantify density of proliferating (BrdU labeled) cells. C. mRNA was extracted from the hippocampus dissected from 12 weeks old *Atxn1*$^{154Q/2Q}$ and wild-type littermate controls (N = 4-6) and RTqPCR was used to evaluate expression of astrocyte specific genes. Data is presented as mean± SEM with average values for each mouse represented by a dot. * p<0.05 Students t-test.

Figure 4. Increased expression of astrocyte homeostatic genes and microglial density in the motor cortex of *Atxn1*$^{154Q/2Q}$ mice. A. Brain sections from 12 weeks old *Atxn1*$^{154Q/2Q}$ and wild-type littermate controls (N = 3-5) were stained for NeuN, GFAP and Iba1. Confocal images of motor cortex were used to quantify density of NeuN positive neurons in layer 6 (B), GFAP expression, cell density and percent area (C-D) and density of Iba1 positive microglia (E-F) in layer 6 and underlying corpus callosum (CC). G-H. mRNA was extracted from the cortex dissected from 12 weeks old *Atxn1*$^{154Q/2Q}$ and wild-type littermate controls (N = 4-6) and RTqPCR was used to evaluate expression of microglial gene *Aif1* (G) and astrocyte specific homeostatic genes (H). Data is presented as mean± SEM with average values for each mouse represented by a dot. * p<0.05 Students t-test.

Figure 5. BDNF expression is decreased in the cerebellum of patients with SCA1. Slices from the cerebellar cortex from the patients with SCA1 and healthy age- and sex- matched controls were stained with GFAP (A) and BDNF (C). B. and E Confocal images were used to quantify molecular layer thickness (B), GFAP expression and area, BDNF% area and puncta density and co-localization of BDNF and GFAP (D). Data is presented as box and whisker plots.* $p<0.05$ Students t-test.

Figure 6. *BDNF* expression is altered in a brain region specific manner early in disease in *Atxn1*$^{154Q/2Q}$ mice. The cerebellum, medulla, cortex and hippocampus were dissected from 12 weeks old *Atxn1*$^{154Q/2Q}$ and wild-type littermate controls (N = 4-6), mRNA was extracted and RTqPCR was used to evaluate expression of *BDNF* mRNA. Data is presented as mean± SEM with average values for each mouse represented by a dot. * $p<0.05$ Students t-test.

Figure 7. BDNF treatment ameliorates motor and cognitive deficits in *Atxn1*$^{154Q/2Q}$ mice. Stereotaxic surgery was used to implant a cannula into a lateral ventricle of 7- week-old *Atxn1*$^{154Q/2Q}$ mice and wild-type littermate controls (N=20 each). Each cannula was connected to the subcutaneous osmotic ALZET pump continuously delivering BDNF or aCSF (N=10) for four weeks. At 11 weeks rotarod and 10 weeks Barnes maze were used to evaluate motor and cognitive performance. A. Latency to fall on rotarod assay. B. Latency to escape during four training days on Barnes maze, C. Strategy development and use during training days of Barnes maze. Data is presented as mean± SEM with average values for each independent experimental sample represented by a dot. * $p<0.05$ Two way ANOVA with post hoc Tukey's testing.

Figure 8. BDNF ameliorates hippocampal neurogenesis and astrocyte gene expression in SCA1 mice.

Stereotaxic surgery was used to implant a cannula into a lateral ventricle of 7- week-old *Atxn1*$^{154Q/2Q}$ mice and wild-type littermate controls. Each cannula was connected to the subcutaneous ALZET pump continuously delivering BDNF or aCSF for four weeks. A–B. At 11 weeks mice were injected with BrdU to label proliferating cells in the hippocampal dentate gyrus. Slices were stained with BrdU antibody (A) and confocal images were used to quantify density of proliferating (BrdU labeled) cells (B). C. Hippocampal slices stained with NeuN were used to evaluate thickness of CA2 and CA3 neuronal cell layers. D. mRNA was extracted from the hippocampus and RTqPCR was used to evaluate expression of astrocyte specific genes. E. GFAP staining and confocal images were used to quantify astrocyte density and intensity og GFAP signal in the hippocampus. Data is presented as mean± SEM with average values for each independent experimental sample represented by a dot. * $p<0.05$, Two way ANOVA with post hoc testing.

Supplementary Figures.

Supplementary Figure 1. Representative image of VGLUT2 and calbindin staining and VGLUT2/ML ratio quantification in the cerebellar molecular layer. Single channel and merged confocal 20um thick images of calbindin and VGLUT2. In merged image, green arrows denote representative measurements of ML width, and white arrows show representative measurements of width of VGLUT2 staining. Images taken in a WT mouse using a 20X objective.

Supplementary Figure 2. Expression of Purkinje cell SCA1 disease associated genes. The cerebellum was dissected from 12 weeks old *Atxn1*$^{154Q/2Q}$ and wild-type littermate controls (N = 4-6), mRNA was extracted and RTqPCR was used to evaluate expression of Purkinje cell

SCA1 disease associated genes. Data is presented as mean± SEM with average values for each independent experimental sample represented by a dot. * p<0.05, Student's t-test.

Supplementary Figure 3. Neuronal density is not altered in deep cerebellar nuclei of 12 weeks old *Atxn1*$^{154Q/2Q}$ mice. A. Cerebellar sections from 12 weeks old *Atxn1*$^{154Q/2Q}$ and wild-type littermate controls (N = 3-5) were stained for NeuN. B-C.Confocal images from each mouse were used to quantify neuronal density in two of deep cerebellar nuclei, the fastigial nucleus (B) and the interposed nucleus (C). Data is presented as mean± SEM with average values for each mouse represented by a dot. * p<0.05 Students t-test.

Supplementary Figure 4. GFAP expression in cerebellar primary fissure. Cerebellar sections from 12 weeks old *Atxn1*$^{154Q/2Q}$ and wild-type littermate controls (N = 3-5) were stained for GFAP (A) and confocal images from each mouse were used to quantify relative fluorescence intensity of GFAP staining in the primary fissure (B). Data is presented as mean± SEM with average values for each mouse represented by a dot. * p<0.05 Students t-test.

Supplementary Figure 5. Expression of astrocyte homeostatic genes is not significantly altered in the cerebellum of 12 weeks old *Atxn1*$^{154Q/2Q}$ mice. mRNA was extracted from the cerebellum dissected from 12 weeks old *Atxn1*$^{154Q/2Q}$ and wild-type littermate controls (N = 4-6) and RTqPCR was used to evaluate expression of astrocyte specific genes. Data is presented as mean± SEM with average values for each mouse represented by a dot. * p<0.05 Student's t-test.

Supplementary Figure 6. Density of microglia is not altered in cerebellar primary fissure. Cerebellar sections from 12 weeks old *Atxn1*$^{154Q/2Q}$ and wild-type littermate controls (N = 3-5) were stained for Iba1 (A) and confocal images from each mouse were used to quantify density

of Iba1 microglia and Iba1 percent area in the primary fissure molecular layer (B) and granule cell layer (C). Data is presented as mean± SEM with average values for each mouse represented by a dot. * p<0.05 Student's t-test.

Supplementary Figure 7. **Changes in area covered by microglia are not detected in medulla.** A. Sections from 12 -week -old wild-type littermate mice (N = 3-5) were stained for microglial marker Iba1. Confocal images from medulla of each mouse were used to measure the percentage of the area occupied by Iba1-stained microglia in medullar inferior olive (A) and medial vestibular nuclei (B). C. mRNA was extracted from the medulla dissected from 12 weeks old *Atxn1*$^{154Q/2Q}$ and wild-type littermate controls (N = 4-6) and RTqPCR was used to evaluate *Aif1* (Iba1) expression. Data is presented as mean± SEM with average values for each mouse represented by a dot. * p<0.05 Students t-test.

Supplementary Figure 8. Hippocampal pathology of neurons, astrocytes and microglia in 12- weeks-old *Atxn1*$^{154Q/2Q}$ mice. Brain sections from 12 weeks old *Atxn1*$^{154Q/2Q}$ and wild-type littermate controls (N = 3-5) were stained for NeuN, GFAP and Iba1. Confocal images were used to quantify thickness (i.e., area divided by length) of CA2 and CA3 (A). Changes in astrocytes were measured by quantifying relative intensity of GFAP staining, astrocytic density, and percent area of GFAP in the granule cell layer of the dentate gyrus (B), and microglial density and area occupied by Iba1 in the hippocampal was quantified both in granule cell layer and hilus of dentate gyrus (C). Data is presented as mean± SEM with average values for each mouse represented by a dot. * p<0.05 Students t-test.

Supplementary Figure 9. Motor and cognitive deficits and failure to gain weight are detectable in 7- weeks-old *Atxn1*$^{154Q/2Q}$ mice. To evaluate behavioral and somatic deficits in

7 -week- old *Atxn1*$^{154Q/2Q}$ and wild-type littermate controls, animals were compared for latency to fall on rotarod assay (A), percentage of time spent freezing in the fear conditioning assay (B), and body weight (C). Data is presented as mean± SEM with average values for each independent experimental sample represented by a dot. * $p<0.05$, Student's t-test.

Supplementary Figure 10. Validation of increased cortical BDNF in BDNF-treated *Atxn1*$^{154Q/2Q}$ and wild-type control mice. BDNF enzyme-linked immunosorbent assay (ELISA) of cerebral tissue of experimental mice (N = 3-7). *P < 0.05 one-way ANOVA with post hoc Tukey's test. Each data point represents individual mouse; bars show the average with error bars = SEM

Supplementary Figure 11. Schematics of six different strategies mice can use to solve Barnes maze. Barnes maze unbiased strategy (BUNS) classification describes six categories of search strategies, which are assigned a decreasing cognitive score: 1) Direct, in which the mouse takes the most efficient path directly to the goal (cognitive score = 1); 2) Corrected, in which the mouse first goes toward one of the holes adjacent to the goal and makes a correction to reach the goal (cognitive score = 0.75); 3) Long correction, in which the mouse first moves toward a hole far from the goal and then turns around and goes directly to the goal (cognitive score = 0.5); 4) Focused search, in which the mouse scans a larger area near the goal (cognitive score = 0.5), 5) Serial, in which the mouse goes around the maze checking each hole in series (cognitive score = 0.25), and 6) Random, in which the mouse takes a long and inefficient path with no obvious pattern (cognitive score = 0).

Supplementary Figure 12. **The effects of BDNF treatment on cognitive performance and body weight of in *Atxn1*$^{154Q/2Q}$ mice and wild-type littermate controls treated with either**

BDNF or aCSF vehicle. Mice were tested via Barnes maze, retested for fear conditioning, and assessed for body weight 3 weeks after onset of chronic BDNF delivery (10 weeks of age). Time spent in goal zone during the Barnes maze probe test (A) and BUNS cognitive score across testing days (B). C. Time spent freezing in the fear conditioning assay. D. Body weight. Data is presented as mean± SEM with average values for each independent experimental sample represented by a dot. * $p<0.05$ Two way ANOVA with post hoc Tukey's testing.

Supplementary Figure 13. **BDNF increases microglial density in the hippocampus of wild-type mice.** 12 weeks old *Atxn1*$^{154Q/2Q}$ and wild-type littermate controls (N = 3-4) were assessed via IHC for changes in microglial density and area covered by Iba1 was determined in granule cell layer (A) and hilus (B) of the hippocampus dentate gyrus. C. Whole-hippocampal tissue was dissected and processed for mRNA extraction. RT-qPCR was used to evaluate expression of *Aif1*, a microglia specific gene. Data is presented as mean± SEM with average values for each mouse represented by a dot. * $p<0.05$ Two-way ANOVA with post hoc Tukey's testing.

Supplementary Figure 14. **Mild beneficial of BDNF in the cerebellar cortex**. Representative images of the molecular layer of the cerebellar cortex co-stained with antibodies for calbindin, VGLUT2, and GFAP (A). Representative images of the granule cell layer and white matter layers of the cerebellar cortex stained with microglial marker Iba1 (B). Purkinje cell health markers molecular layer thickness and VGLUT2/ML ratio (C) as well as percent area covered by GFAP staining (D) were assessed in the molecular layer of the cerebellum. Microglia density in the white matter layer of the cerebellar cortex was assessed using the marker Iba1 (E). Whole-cerebellar mRNA was extracted, and RT-qPCR was used to evaluate expression of Purkinje cell SCA1 disease associated genes (F). Extracted mRNA was also used to evaluate expression of astrocyte homeostatic genes (G) and the microglia-specific gene *Aif1* (H). Data is presented as

mean± SEM with average values for each independent experimental sample represented by a dot. * p<0.05, Two way ANOVA with post hoc Tukey's testing.

Supplementary Figure 15. **The effect of BDNF on the neurons, astrocytes and microglia of the medulla**. Representative images of NeuN neuronal marker in the medial vestibular nucleus (A), GFAP astrocyte marker in the inferior olive nucleus (B), and Iba1 microglia marker in the medial vestibular nucleus (C) of the medulla oblongata. Quantification of NeuN stained cells in the lateral reticulate and medial vestibular nuclei of the medulla (D). Quantification of astrocyte density and relative intensity of GFAP staining in the inferior olive (E). Quantification of microglial density and area of Iba1 staining in the inferior olive and medial vestibular nuclei of the medulla (F). Whole-medulla mRNA was extracted, and RT-qPCR was used to evaluate expression of astrocyte homeostatic genes (G) and the microglia-specific gene *Aif1* (H). Data is presented as mean± SEM with average values for each independent experimental sample represented by a dot. * p<0.05, Two way ANOVA with post hoc Tukey's testing.

Supplementary Figure 16. **The effect of BDNF on the neurons, astrocytes and microglia of the cortex**. Representative images of NeuN neuronal marker in the motor cortex layers 5-6 as well as GFAP and Iba1 markers of microglia and astrocytes respectively in layer 6 and the corpus callosum of the motor cortex (A). Quantification of density of NeuN stained cells in motor cortex layers 5-6 (B). Quantification of intensity of GFAP staining, percent area covered by GFAP staining, and astrocyte density in layer 6 of the motor cortex as well as in the underlying corpus callosum (C). Quantification of microglial density and percent area covered by Iba1 staining in layer 6 of the motor cortex and in the underlying corpus callosum (D). Whole-cortex mRNA was extracted, and RT-qPCR was used to evaluate expression of astrocyte homeostatic genes (F) and the microglia-specific gene *Aif1* (G). Data is presented as mean± SEM with

average values for each independent experimental sample represented by a dot. * $p<0.05$, Two way ANOVA with post hoc Tukey's testing.

1. Zoghbi HY, Orr HT. Pathogenic mechanisms of a polyglutamine-mediated neurodegenerative disease, Spinocerebellar ataxia type 1. J. Biol. Chem. 2009;284:7425–9.

2. I. K, M. M, T. S-H, M. H, T. K, U. W, et al. Neuropsychological features of patients with spinocerebellar ataxia (SCA) types 1, 2, 3, and 6. Cerebellum. 2010;9:433–42.

3. Zoghbi HY, Pollack MS, Lyons SLA, Ferrell TRE, Daiger SP, Beaudet AL. Spinocerebellar Ataxia□: Variable Age of Onset and Linkage to Human Leukocyte Antigen in a Large Kindred. Ann. Neurol. 1988;23:580–4.

4. Koeppen AH. The pathogenesis of spinocerebellar ataxia. The cerebellum. 2005;4:62–73.

5. Friedrich J, Henzler C, Orr HT, Friedrich J, Kordasiewicz HB, Callaghan BO, et al. Antisense oligonucleotide–mediated ataxin-1 reduction prolongs survival in SCA1 mice and reveals disease-associated transcriptome profiles. J. Clin. Investig. 2018;3.

6. Rüb U, Bürk K, Timmann D, den Dunnen W, Seidel K, Farrag K, et al. Spinocerebellar ataxia type 1 (SCA1): New pathoanatomical and clinico-pathological insights. Neuropathol. Appl. Neurobiol. 2012;38:665–80.

7. Seidel K, Siswanto S, Brunt ERP. Brain pathology of spinocerebellar ataxias. Acta Neuropathol. 2012;124:1–21.

8. Diallo A, Jacobi H, Cook A, Giunti P, Parkinson MH, Labrum R, et al. Prediction of Survival With Long-Term Disease Progression in Most Common Spinocerebellar Ataxia. Mov. Disord. 2019;34:1220–7.

9. Moriarty A, Cook A, Hunt H, Adams ME, Cipolotti L, Giunti P. A longitudinal investigation into cognition and disease progression in spinocerebellar ataxia types 1, 2, 3, 6, and 7. Orphanet J. Rare Dis. [Internet]. Orphanet Journal of Rare Diseases; 2016;11:82. Available from: http://dx.doi.org/10.1186/s13023-016-0447-

6%5Cnhttp://www.ncbi.nlm.nih.gov/pubmed/27333979%5Cnhttp://www.pubmedcentral.nih.gov/articlerender.fcgi?artid=PMC4917932

10. Jacobi H, Reetz K, du Montcel ST, Bauer P, Mariotti C, Nanetti L, et al. Biological and clinical characteristics of individuals at risk for spinocerebellar ataxia types 1, 2, 3, and 6 in the longitudinal RISCA study: Analysis of baseline data. Lancet Neurol. 2013;12:650–8.

11. Koscik TR, Sloat L, Plas E Van Der, Joers JM, Deelchand DK, Lenglet C. Brainstem and striatal volume changes are detectable in under 1 year and predict motor decline in spinocerebellar ataxia type 1. Brain Commun. 2020;2:1–13.

12. Seidel K, Siswanto S, Brunt ERP, Den Dunnen W, Korf HW, Rüb U. Brain pathology of spinocerebellar ataxias. Acta Neuropathol. 2012;124:1–21.

13. Rüb U, Schöls L, Paulson H, Auburger G, Kermer P, Jen JC, Seidel K, Korf HW DT. Clinical features, neurogenetics and neuropathology of the polyglutamine spinocerebellar ataxias type 1, 2, 3, 6 and 7. Prog. Neurobiol. 2013;104:38–66.

14. Watase K, Weeber EJ, Xu B, Antalffy B, Yuva-Paylor L, Hashimoto K, et al. A long CAG repeat in the mouse Sca1 locus replicates SCA1 features and reveals the impact of protein solubility on selective neurodegeneration. Neuron. 2002;34:905–19.

15. Asher M, Rosa J, Rainwater O, Duvick L, Bennyworth M, Lai R, et al. Cerebellar contribution to the cognitive alterations in SCA1□: evidence from mouse models. Hum Mol Genet. 2020;29:117–31.

16. Suh J, Romano DM, Nitschke L, Albers MW, Zoghbi HY, Tanzi RE, et al. Loss of Ataxin-1 Potentiates Alzheimer ' s Pathogenesis by Elevating Cerebral BACE1 Transcription. Cell. 2019;178:1159–75.

17. Cvetanovic M, Hu YS, Opal P. Mutant Ataxin-1 Inhibits Neural Progenitor Cell Proliferation in SCA1. Cerebellum [Internet]. The Cerebellum; 2016;1–8. Available from: http://dx.doi.org/10.1007/s12311-016-0794-9

18. Nwaobi SE, Cuddapah VA, Patterson KC, Randolph AC, Olsen ML. The role of glial □

specific Kir4 . 1 in normal and pathological states of the CNS. Acta Neuropathol. Springer Berlin Heidelberg; 2016;132:1–21.

19. Nagelhus EA, Ottersen OP. Physiological roles of Aquaporin-4 in brain. Physiol. Rev. 2013;93:1543–62.

20. Rothstein J, Dykes-Hoberg M, Pardo C, Bristol L, Jin L, Kuncl R, et al. Antisense knockout of glutamate transporters reveals a predominant role for astroglial glutamate transport in excitotoxicity and clearance of extracellular glutamate. Neuron [Internet]. 1996;16:675–86. Available from: papers2://publication/uuid/327F682D-2D03-48C7-A0E6-A57E2CD92157

21. Cycle W, Clasadonte J, Scemes E, Wang Z, Boison D, Haydon PG, et al. Connexin 43-Mediated Astroglial Metabolic Networks Contribute to the Regulation of the Sleep- Connexin 43-Mediated Astroglial Metabolic Networks Contribute to the Regulation of the Sleep-Wake Cycle. Neuron [Internet]. Elsevier Inc.; 2017;1–16. Available from: http://dx.doi.org/10.1016/j.neuron.2017.08.022

22. Mellesmoen A, Sheeler C, Ferro A, Rainwater O, Cvetanovic M. Brain Derived Neurotrophic Factor (BDNF) Delays Onset of Pathogenesis in Transgenic Mouse Model of Spinocerebellar Ataxia Type 1 (SCA1). Front. Cell. Neurosci. 2019;12:1–8.

23. Sheeler C, Rosa J, Borgenheimer E, Mellesmoen A, Rainwater O. Post-symptomatic Delivery of Brain-Derived Neurotrophic Factor (BDNF) Ameliorates Spinocerebellar Ataxia Type 1 (SCA1) Pathogenesis. The Cerebellum. The Cerebellum; 2021;1.

24. Gatchel JR, Zoghbi HY. Diseases of unstable repeat expansion: mechanisms and common principles. Nat. Rev. Genet. 2005;6:743–55.

25. National Research Council (US) Committee for the Update of the Guide for the Care and Use of Laboratory Animals. Guide for the Care and Use of Laboratory Animals, 8th edition. 2011.

26. Illouz T, Madar R, Clague C, Griffioen KJ, Louzoun Y, Okun E, et al. Unbiased classification of spatial strategies in the Barnes maze. Bioinformatics. 2016;32:3314–20.

27. Ferro A, Qu W, Lukowicz A, Svedberg D, Johnson A, Cvetanovic M. Inhibition of NF-κB signaling in IKKβ F/F;LysM Cre mice causes motor deficits but does not alter pathogenesis of Spinocerebellar ataxia type 1. PLoS One. 2018;1:1–21.

28. Asher M, Johnson A, Zecevic B, Pease D, Cvetanovic M. Ataxin-1 regulates proliferation of hippocampal neural precursors. Neuroscience. IBRO; 2016;322:54–65.

29. Kim JH, Lukowicz A, Qu W, Johnson A, Cvetanovic M. Astroglia contribute to the pathogenesis of spinocerebellar ataxia Type 1 (SCA1) in a biphasic , stage-of-disease specific manner. Glia. 2018;1–16.

30. Asher M, Johnson A, Zecevic B, Pease D, Cvetanovic M. Ataxin-1 regulates proliferation of hippocampal neural precursors. Neuroscience [Internet]. IBRO; 2016;322:54–65. Available from: http://dx.doi.org/10.1016/j.neuroscience.2016.02.011

31. Dunn KW, Kamocka MM, McDonald JH. A practical guide to evaluating colocalization in biological microscopy. Am. J. Physiol. - Cell Physiol. 2011;300:723–42.

32. Kim JH, Lukowicz A, Qu W, Johnson A, Cvetanovic M. Astroglia contribute to the pathogenesis of spinocerebellar ataxia Type 1 (SCA1) in a biphasic, stage-of-disease specific manner. Glia. 2018;66:1972–87.

33. Nigri A, Sarro L, Mongelli A, Castaldo A, Porcu L, Pinardi C, et al. Spinocerebellar Ataxia Type 1□: One □ Year Longitudinal Study to Identify Clinical and MRI Measures of Disease Progression in Patients and Presymptomatic Carriers. The Cerebellum [Internet]. Springer US; 2021; Available from: https://doi.org/10.1007/s12311-021-01285-0

34. Ebner B, Ingram MA, Barnes JA, Duvick LA, Frisch JL, Clark HB, et al. Purkinje cell ataxin-1 modulates climbing fiber synaptic input in developing and adult mouse cerebellum. J. Neurosci. [Internet]. 2013;33:5806–20. Available from: http://www.ncbi.nlm.nih.gov/pubmed/23536093

35. Duvick L, Barnes J, Ebner B, Agrawal S, Andresen M, Lim J, et al. SCA1-like disease in mice expressing wild-type Ataxin-1 with a serine to aspartic acid replacement at residue 776. Neuron [Internet]. Elsevier Inc.; 2010;67:929–35. Available from:

http://dx.doi.org/10.1016/j.neuron.2010.08.022

36. Ingram M, Wozniak EAL, Duvick L, Zoghbi HY, Henzler C, Orr HT. Cerebellar Transcriptome Profiles of ATXN1 Transgenic Mice Reveal SCA1 Disease Progression and Protection Pathways Article Cerebellar Transcriptome Profiles of ATXN1 Transgenic Mice Reveal SCA1 Disease Progression and Protection Pathways. Neuron [Internet]. Elsevier Inc.; 2016;89:1194–207. Available from: http://dx.doi.org/10.1016/j.neuron.2016.02.011

37. Sillitoe R V, Fu Y, Watson C. Cerebellum [Internet]. Mouse Nerv. Syst. Elsevier Inc.; 2012. Available from: http://dx.doi.org/10.1016/B978-0-12-369497-3.10011-1

38. Lippman Bell JJ, Lordkipanidze T, Cobb N, Dunaevsky A. Bergmann glial ensheathment of dendritic spines regulates synapse number without affecting spine motility. Neuron Glia Biol. 2010;6:193–200.

39. Farmer WT, Chierzi S, Lui C, Zaelzer C, Jones E V, Bally BP, et al. Neurons diversify astrocytes in the adult brain through sonic hedgehog signaling. Science (80-.). 2016;351.

40. Escartin C, Carmignoto G, Agarwal A, Allen NJ, Araque A, Barbeito L, et al. Reactive astrocyte nomenclature, definitions, and future directions. Nat Neurosci. 2021;

41. Pekny M, Pekna M, Messing A, Steinhäuser C, Lee JM, Parpura V, Hol EM, Sofroniew MV VA. Astrocytes: a central element in neurological diseases. Acta Neuropathol. 2016;131:323–45.

42. Cvetanovic M, Ingram M, Orr H, Opal P. Early activation of microglia and astrocytes in mouse models of spinocerebellar ataxia type 1. Neuroscience [Internet]. IBRO; 2015;289:289–99. Available from: http://linkinghub.elsevier.com/retrieve/pii/S0306452215000159

43. Verkhratsky, Alexei Nedergaard M. Physiology of Astroglia. Physiol Rev. 2018;98:239–389.

44. Perea G, Sur M, Araque A. Neuron-glia networks: integral gear of brain function. Front. Cell. Neurosci. [Internet]. 2014;8:378. Available from: http://www.pubmedcentral.nih.gov/articlerender.fcgi?artid=4222327&tool=pmcentrez&rendertype=abstract

45. Kofuji P, Newman EA. Potassium buffering in the central nervous system. Neuroscience. 2004;129:1045–56.

46. Djukic B, Kristen B. Casper, Benjamin D. Philpot, Lih-Shen Chin and KDM. Conditional Knock-Out of Kir4.1 Leads to Glial Membrane Depolarization, Inhibition of Potassium and Glutamate Uptake, and Enhanced Short-Term Synaptic Potentiation. J. Neurosci. 2007;27:11354–65.

47. Mellesmoen A, Sheeler C, Ferro A, Rainwater O, Cvetanovic M. Brain derived neurotrophic factor (BDNF) delays onset of pathogenesis in transgenic mouse model of spinocerebellar ataxia type 1 (SCA1). Front. Cell. Neurosci. 2018;

48. Qu W, Johnson A, Kim JH, Lukowicz A, Svedberg D, Cvetanovic M. Inhibition of colony-stimulating factor 1 receptor early in disease ameliorates motor deficits in SCA1 mice. J. Neuroinflammation. Journal of Neuroinflammation; 2017;14:1–11.

49. Banfi S, Servadio A, Chung M, Capozzoli F, Duvick L, Elde R, et al. Cloning and developmental expression analysis of the murine homolog of the spinocerebellar ataxia type 1 gene (Sca1). Hum. Mol. Genet. 1996;5:33–40.

50. Rüb U, Schöls L, Paulson H, Auburger G, Kermer P, Jen JC, et al. Clinical features, neurogenetics and neuropathology of the polyglutamine spinocerebellar ataxias type 1, 2, 3, 6 and 7. Prog. Neurobiol. 2013.

51. Jacobi H, Tezenas S, Bauer P, Giunti P, Cook A, Labrum R. Long-term evolution of patient-reported outcome measures in spinocerebellar ataxias. J. Neurol. [Internet]. Springer Berlin Heidelberg; 2018;265:2040–51. Available from: http://dx.doi.org/10.1007/s00415-018-8954-0

52. Kish SJ, El-awar ISM, Schut L, Leach L, Oscar-berrnan M, Freedman M. Cognitive Deficits in Olivopontocerebellar Atrophy□: Implications for the Cholinergic Hypothesis of Alzheimer ' s Dementia. Ann Neurol. 1988;24:200–6.

53. Moriarty A, Cook A, Hunt H, Adams ME, Cipolotti L, Giunti P. A longitudinal investigation into cognition and disease progression in spinocerebellar ataxia types 1 , 2 , 3 , 6 , and 7.

Orphanet J. Rare Dis. [Internet]. Orphanet Journal of Rare Diseases; 2016;1–9. Available from: http://dx.doi.org/10.1186/s13023-016-0447-6

54. Ma J, Wu C, Lei J, Zhang X. Cognitive impairments in patients with spinocerebellar ataxia types 1 , 2 and 3 are positively correlated to the clinical severity of ataxia symptoms. Int J Cli Exp Med. 2014;7:5765–71.

55. Bürk K, Globas C, Bösch S, Klockgether T, Zühlke C, Daum I, et al. Cognitive deficits in spinocerebellar ataxia type 1, 2, and 3. J. Neurol. 2003;250:207–11.

56. Fancellu R, Paridi D, Tomasello C, Panzeri M, Castaldo A, Genitrini S, et al. Longitudinal study of cognitive and psychiatric functions in spinocerebellar ataxia types 1 and 2. J. Neurol. Springer Berlin Heidelberg; 2013;260:3134–43.

57. Andreska T, Aufmkolk S, Sauer M, Blum R. High abundance of BDNF within glutamatergic presynapses of cultured hippocampal neurons. Front. Cell. Neurosci. 2014;8:1–15.

58. Burright EN, Clark HB, Servadio a, Matilla T, Feddersen RM, Yunis WS, et al. SCA1 transgenic mice: a model for neurodegeneration caused by an expanded CAG trinucleotide repeat. Cell. 1995;82:937–48.

59. Pelleymounte M, Cullen M, WellNman C. Characteristics of BDNF-induced weight loss. Exp Neurol. 1995;131:229–38.

60. Lee J, Duan W, Mattson MP. Evidence that brain-derived neurotrophic factor is required for basal neurogenesis and mediates , in part , the enhancement of neurogenesis by dietary restriction in the hippocampus of adult mice. 2002;1367–75.

61. Ha S, Vismitha B, David R, Wei Y, Dong F, Jo G, et al. Intermittent fasting increases adult hippocampal neurogenesis. 2020;1–6.

62. Choi SH, Bylykbashi E, Chatila ZK, Lee SW, Pulli B, Clemenson GD, et al. Combined adult neurogenesis and BDNF mimic exercise effects on cognition in an Alzheimer’s mouse model. Science (80-.). 2018;

63. Amato LC, Speranza L, Volpicelli F. Neurotrophic Factor BDNF , Physiological Functions

and Therapeutic Potential in Depression , Neurodegeneration and Brain Cancer. :1–29.
64. Quesseveur G, David DJ, Gaillard MC, Pla P, Wu M V, Nguyen HT, et al. BDNF overexpression in mouse hippocampal astrocytes promotes local neurogenesis and elicits anxiolytic-like activities. 2013;
65. Holt LM, Hernandez RD, Pacheco NL, Torres Ceja B, Hossain M, Olsen ML. Astrocyte morphogenesis is dependent on BDNF signaling via astrocytic TrkB.T1. Elife. 2019;8:1–27.
66. Fernández-García S, Sancho-Balsells A, Longueville S, Hervé D, Gruart A, Delgado-García JM, et al. Astrocytic BDNF and TrkB regulate severity and neuronal activity in mouse models of temporal lobe epilepsy. Cell Death Dis. [Internet]. Springer US; 2020;11. Available from: http://dx.doi.org/10.1038/s41419-020-2615-9
67. Soreq L, Brain UKC, North American BE, Rose J, Patani R, Ule J. Major Shifts in Glial Regional Identity Are a Transcriptional Hallmark of Human Brain Aging. CellReports [Internet]. ElsevierCompany.; 2017;18:557–70. Available from: http://dx.doi.org/10.1016/j.celrep.2016.12.011
68. Yu X, Nagai J, Marti-Solano M, Soto JS, Coppola G, Babu MM, et al. Context-Specific Striatal Astrocyte Molecular Responses Are Phenotypically Exploitable. Neuron [Internet]. Elsevier Inc.; 2020;108:1146-1162.e10. Available from: https://doi.org/10.1016/j.neuron.2020.09.021
69. Miyazaki T, Yamasaki M, Hashimoto K, Kohda K, Yuzaki M, Shimamoto K, et al. Glutamate transporter GLAST controls synaptic wrapping by Bergmann glia and ensures proper wiring of Purkinje cells. Proc. Natl. Acad. Sci. [Internet]. 2017;114:7438–43. Available from: http://www.pnas.org/lookup/doi/10.1073/pnas.1617330114
70. Tong X, Ao Y, Faas GC, Nwaobi SE, Xu J, Haustein MD, et al. Astrocyte Kir4.1 ion channel deficits contribute to neuronal dysfunction in Huntington's disease model mice. Nat. Neurosci. [Internet]. 2014;17:694–703. Available from: http://www.ncbi.nlm.nih.gov/pubmed/24686787
71. Kelley KW, Haim L Ben, Schirmer L, Lakatos A, Ullian EM, Rowitch DH, et al. Kir4.1-

Dependent Astrocyte-Fast Motor Neuron Interactions Are Required for Peak Strength. Neuron [Internet]. Elsevier Inc.; 2018;1–14. Available from: https://doi.org/10.1016/j.neuron.2018.03.010

72. Cui Y, Yang Y, Ni Z, Dong Y, Cai G, Foncelle A, et al. Astroglial Kir4.1 in the lateral habenula drives neuronal bursts in depression. Nature [Internet]. Nature Publishing Group; 2018;554:323–7. Available from: http://www.nature.com/doifinder/10.1038/nature25752

73. Liu E, Peng X, Ma H, Zhang Y, Yang X, Zhang Y. The Involvement of Aquaporin-4 in the Interstitial Fluid Drainage Impairment Following Subarachnoid Hemorrhage. Front. Aging Neurosci. 2021;12:1–11.

74. Matute C, Domercq M, Sánchez-Gómez M-V. Glutamate-mediated glial injury: Mechanisms and clinical importance. Glia [Internet]. 2006;53:212–24. Available from: http://doi.wiley.com/10.1002/glia.20275

75. Pardo AC, Wong V, Benson LM, Dykes M, Tanaka K, Rothstein JD, et al. Loss of the astrocyte glutamate transporter GLT1 modifies disease in SOD1G93A mice. Exp. Neurol. 2006;201:120–30.

76. Mcloughlin HS, Moore LR, Chopra R, Komlo R, Mckenzie M, Blumenstein KG, et al. Oligonucleotide Therapy Mitigates Disease in Spinocerebellar Ataxia Type 3 Mice. Ann. Clin. Transl. Neurol. 2018;84:64–77.

77. Sheeler C, Rosa J, Ferro A, Mcadams B, Borgenheimer E, Cvetanovic M. Glia in Neurodegeneration□: The Housekeeper , the Defender and the Perpetrator. Int. J. Mol. Sci. 2020;21:1–16.

78. Miranda M, Morici JF, Zanoni MB, Bekinschtein P. Brain-Derived Neurotrophic Factor□: A Key Molecule for Memory in the Healthy and the Pathological Brain. Front. Cell. Neurosci. 2019;13:1–25.

79. Gharami K, Xie Y, Ji An J, Tonegawa S, Xu B. Brain-derived Neurotrophic Factor Over-expression in the Forebrain Ameliorates Huntington's Disease Phenotypes in Mice. J Neurochem. 2008;105:369–79.

80. Xie Y, Hayden MR, Xu B. Neurobiology of Disease BDNF Overexpression in the Forebrain Rescues Huntington ' s Disease Phenotypes in YAC128 Mice. J. Neurosci. 2010;30:14708–18.

81. Canals JM, Pineda JR, Torres-Peraza JF, Bosch M, Martín-Ibañez R, Muñoz MT, et al. Brain-derived neurotrophic factor regulates the onset and severity of motor dysfunction associated with enkephalinergic neuronal degeneration in Huntington's disease. J. Neurosci. 2004;24:7727–39.

82. Nagahara AH, Merrill DA, Coppola G, Tsukada S, Schroeder BE, Shaked GM, et al. Neuroprotective effects of brain-derived neurotrophic factor in rodent and primate models of Alzheimer's disease. Nat. Med. [Internet]. 2009;15:331–7. Available from: http://www.pubmedcentral.nih.gov/articlerender.fcgi?artid=2838375&tool=pmcentrez&rendertype=abstract

83. Tsukahara T, Takeda M, Shimohama S, Ohara O HN. Effects of brain-derived neurotrophic factor on 1-methyl-4-phenyl-1,2,3,6-tetrahydropyridine-induced parkinsonism in monkeys. Neurosurgery. 1995;37:733–9.

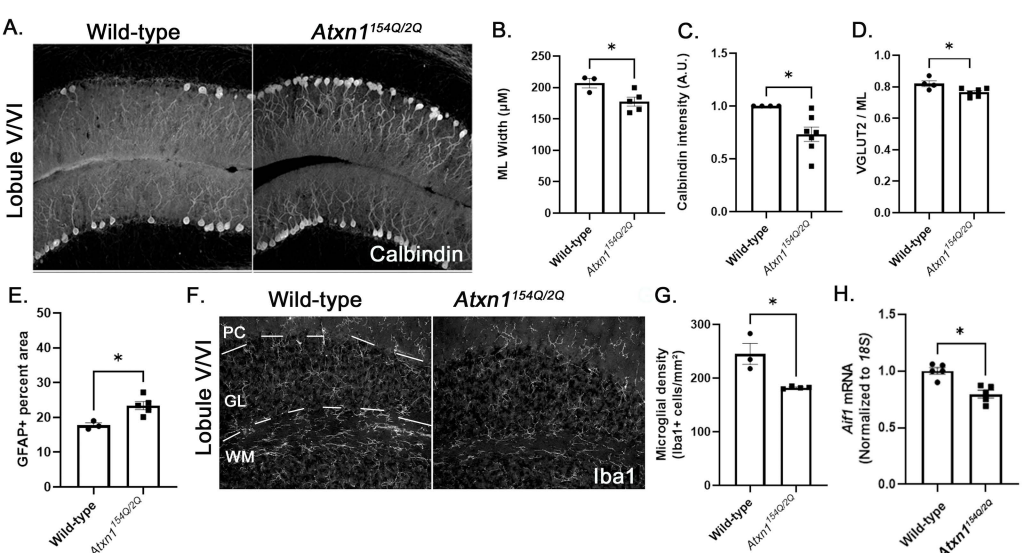
A.
Wild-type
Atxn1 154Q/2Q
Lobule V/VI
Calbindin
B.
ML Width (μM)
250
200
150
100
50
0
*
Wild-type
Atxn1 154Q/2Q
C.
Calbindin intensity (A.U.)
1.5
1.0
0.5
0.0
*
Wild-type
Atxn1 154Q/2Q
D.
VGLUT2 / ML
1.0
0.8
0.6
0.4
0.2
0.0
*
Wild-type
Atxn1 154Q/2Q
E.
GFAP+ percent area
50
40
30
20
10
0
*
Wild-type
Atxn1 154Q/2Q
F.
Wild-type
Atxn1 154Q/2Q
Lobule V/VI
PC
GL
WM
Iba1
G.
Microglial density
(Iba1+ cells/mm²)
300
200
100
0
*
Wild-type
Atxn1 154Q/2Q
H.
Aif1 mRNA
(Normalized to 18S)
1.5
1.0
0.5
0.0
*
Wild-type
Atxn1 154Q/2Q

Figure 1.

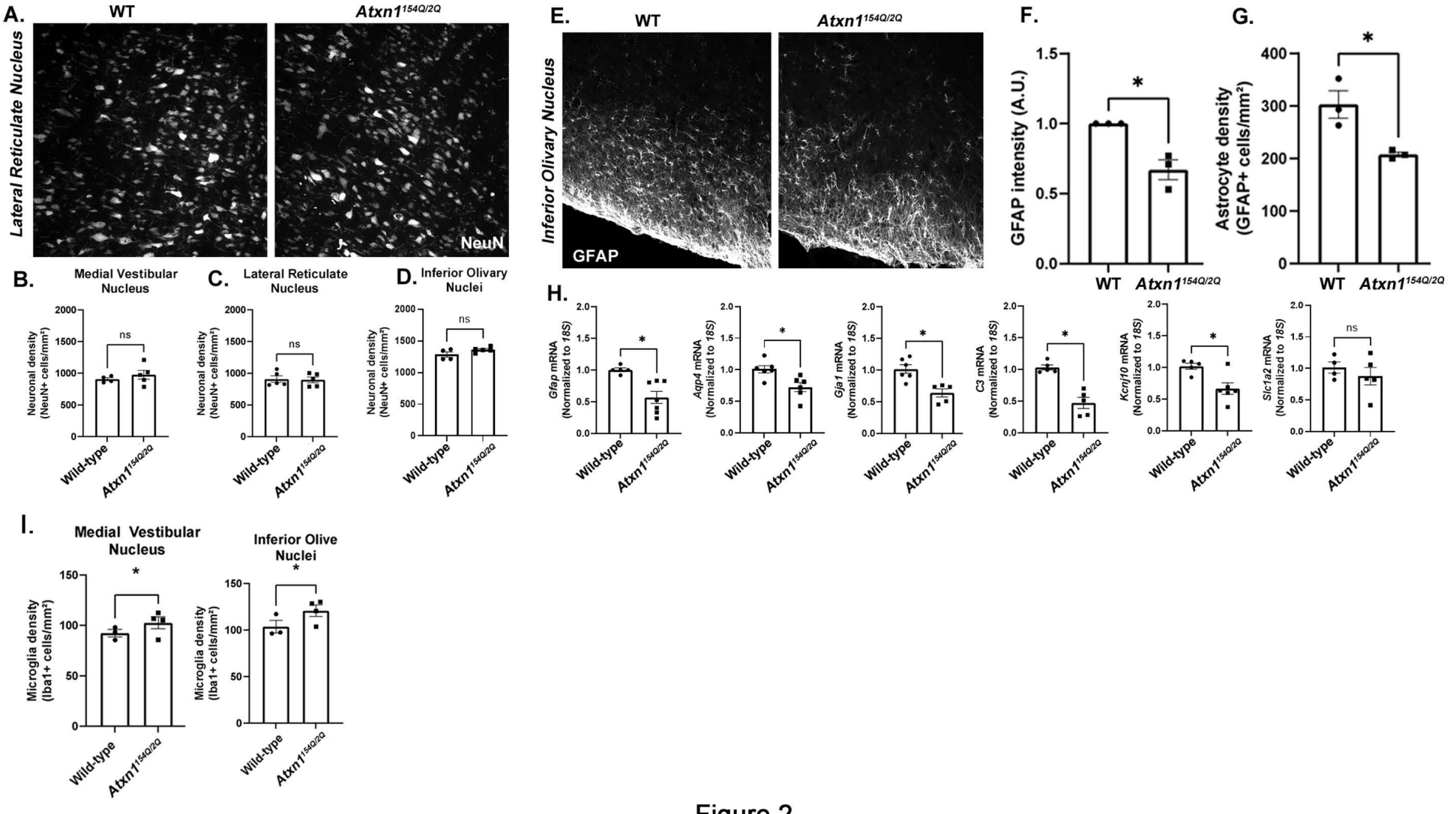
A.
WT
Atxn1154Q/2Q
Lateral Reticulate Nucleus
NeuN
B.
Medial Vestibular Nucleus
C.
Lateral Reticulate Nucleus
D.
Inferior Olivary Nuclei
Neuronal density (NeuN+ cells/mm²)
ns
Wild-type
Atxn1154Q/2Q
E.
WT
Atxn1154Q/2Q
Inferior Olivary Nucleus
GFAP
F.
GFAP intensity (A.U.)
*
WT
Atxn1154Q/2Q
G.
Astrocyte density (GFAP+ cells/mm²)
*
WT
Atxn1154Q/2Q
H.
Gfap mRNA (Normalized to 18S)
Aqp4 mRNA (Normalized to 18S)
Gja1 mRNA (Normalized to 18S)
C3 mRNA (Normalized to 18S)
Kcnj10 mRNA (Normalized to 18S)
Slc1a2 mRNA (Normalized to 18S)
ns
Wild-type
Atxn1154Q/2Q
I.
Medial Vestibular Nucleus
Inferior Olive Nuclei
Microglia density (Iba1+ cells/mm²)
*
Wild-type
Atxn1154Q/2Q

Figure 2.

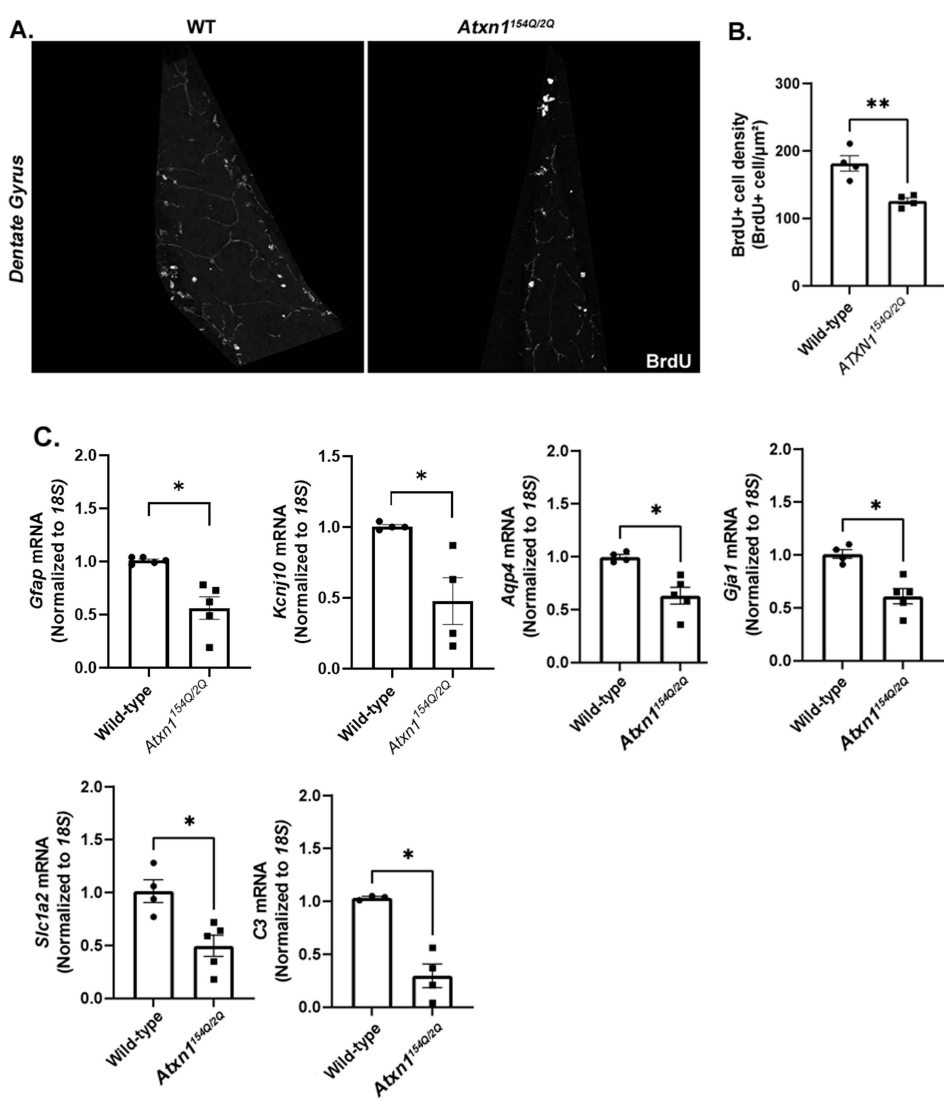
A.
WT
Atxn1154Q/2Q
Dentate Gyrus
BrdU
B.
BrdU+ cell density
(BrdU+ cell/μm²)
300
200
100
0
**
Wild-type
ATXN1 154Q/2Q
C.
Gfap mRNA
(Normalized to 18S)
Kcnj10 mRNA
(Normalized to 18S)
Aqp4 mRNA
(Normalized to 18S)
Gja1 mRNA
(Normalized to 18S)
Slc1a2 mRNA
(Normalized to 18S)
C3 mRNA
(Normalized to 18S)
2.0
1.5
1.0
0.5
0.0
*
Wild-type
Atxn1154Q/2Q

Figure 3.

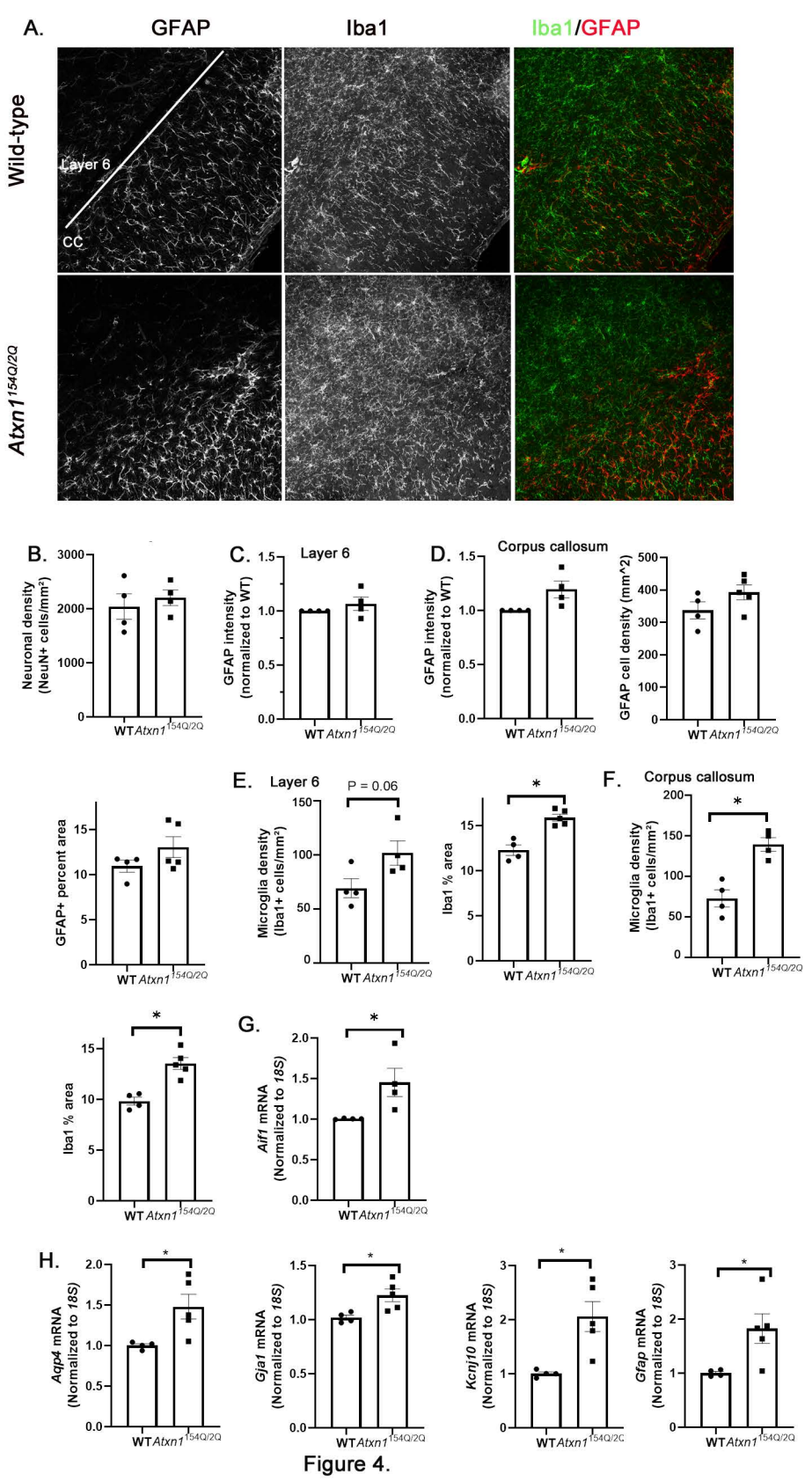
A.
GFAP
Iba1
Iba1/GFAP
Wild-type
Atxn1 154Q/2Q
Layer 6
CC
B.
Neuronal density (NeuN+ cells/mm²)
C.
Layer 6
GFAP intensity (normalized to WT)
D.
Corpus callosum
GFAP intensity (normalized to WT)
GFAP cell density (mm^2)
WT
Atxn1 154Q/2Q
GFAP+ percent area
E.
Layer 6
P = 0.06
Microglia density (Iba1+ cells/mm²)
Iba1 % area
F.
Corpus callosum
Microglia density (Iba1+ cells/mm²)
Iba1 % area
G.
Aif1 mRNA (Normalized to 18S)
H.
Aqp4 mRNA (Normalized to 18S)
Gja1 mRNA (Normalized to 18S)
Kcnj10 mRNA (Normalized to 18S)
Gfap mRNA (Normalized to 18S)

Figure 4.

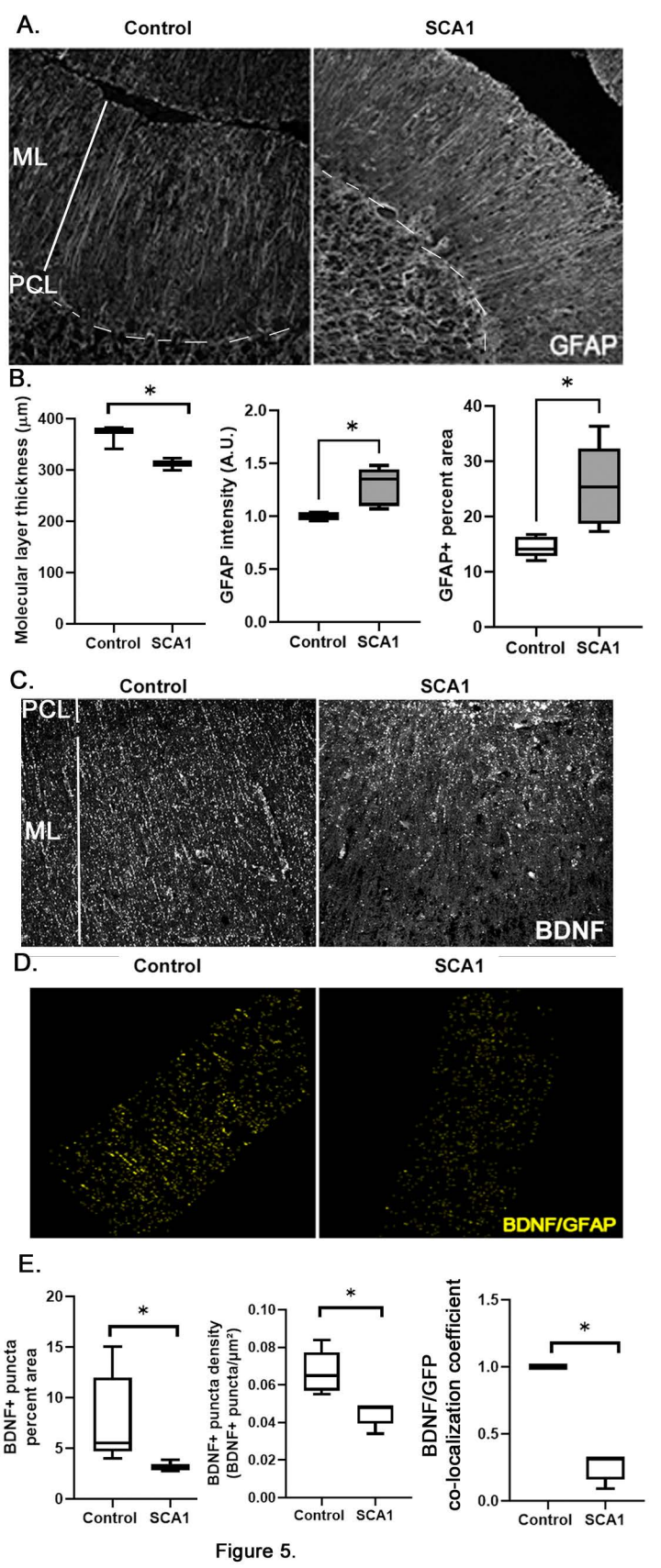
A.
Control
SCA1
ML
PCL
GFAP
B.
Molecular layer thickness (µm)
400
300
200
100
0
Control
SCA1
GFAP intensity (A.U.)
2.0
1.5
1.0
0.5
0.0
GFAP+ percent area
40
30
20
10
C.
BDNF
D.
BDNF/GFAP
E.
BDNF+ puncta percent area
20
15
10
5
BDNF+ puncta density (BDNF+ puncta/µm²)
0.10
0.08
0.06
0.04
0.02
0.00
BDNF/GFP co-localization coefficient
1.5
1.0
0.5
0.0

Figure 5.

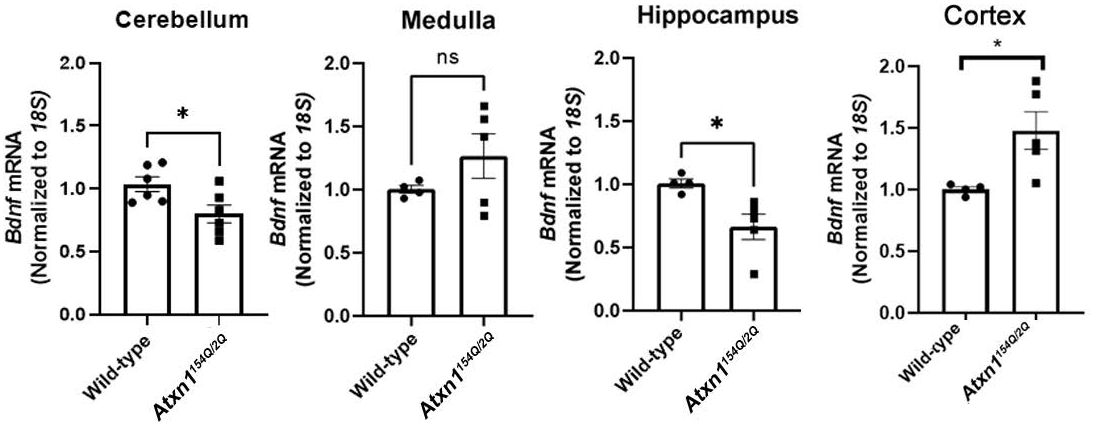
Cerebellum
Medulla
Hippocampus
Cortex
Bdnf mRNA
(Normalized to 18S)
2.0
1.5
1.0
0.5
0.0
*
ns
Wild-type
Atxn1154Q/2Q

Figure 6.

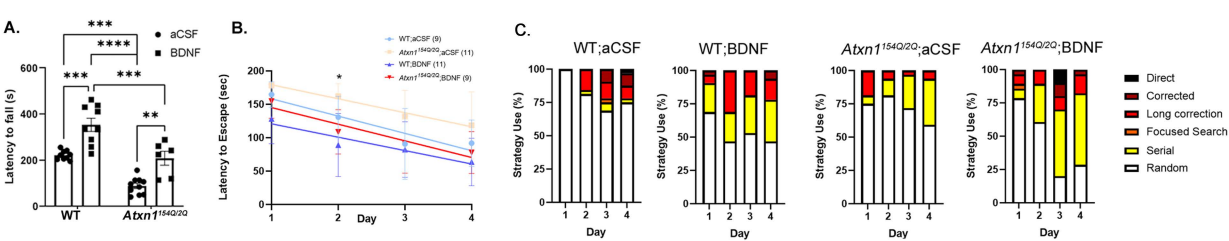
A.
aCSF
BDNF
Latency to fall (s)
WT
Atxn1154Q/2Q
B.
WT;aCSF (9)
Atxn1154Q/2Q;aCSF (11)
WT;BDNF (11)
Atxn1154Q/2Q;BDNF (9)
Latency to Escape (sec)
Day
C.
WT;aCSF
WT;BDNF
Atxn1154Q/2Q;aCSF
Atxn1154Q/2Q;BDNF
Strategy Use (%)
Day
Direct
Corrected
Long correction
Focused Search
Serial
Random

Figure 7.

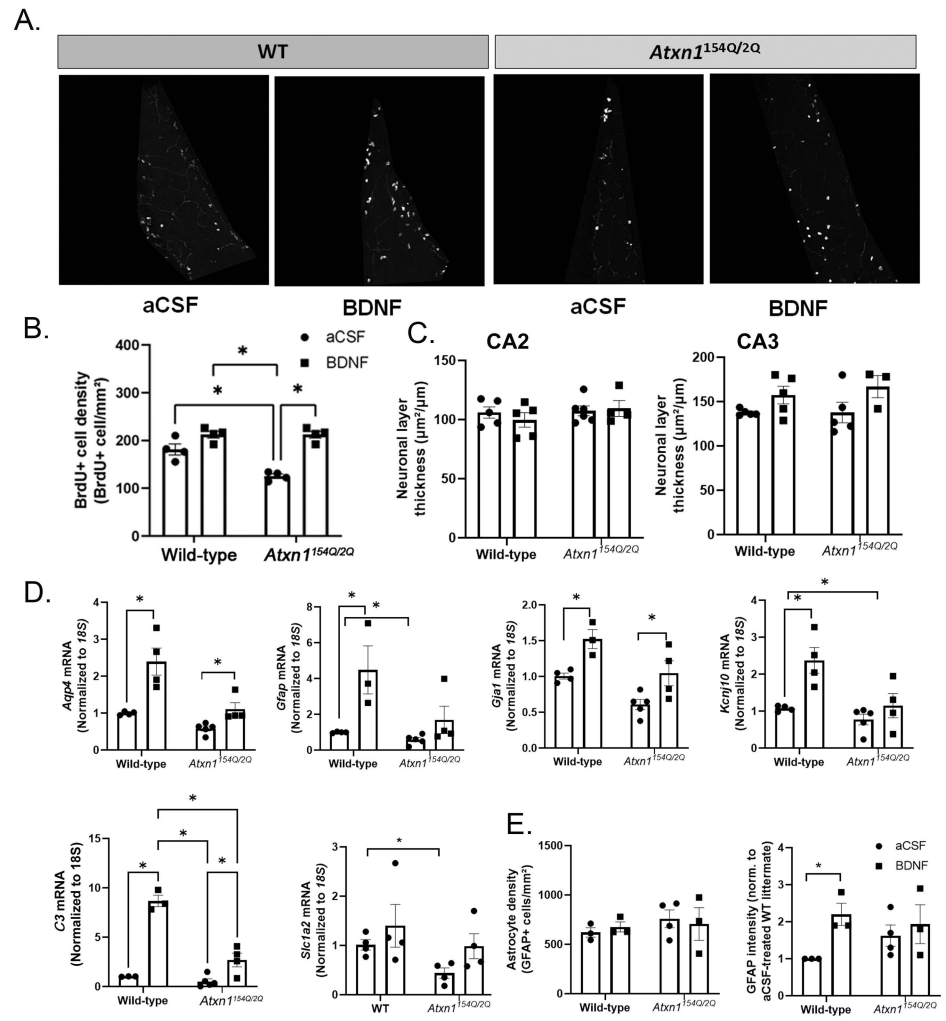
A.
WT
Atxn1154Q/2Q
aCSF
BDNF
aCSF
BDNF
B.
aCSF
BDNF
BrdU+ cell density (BrdU+ cell/mm²)
Wild-type
Atxn1154Q/2Q
C.
CA2
CA3
Neuronal layer thickness (µm²/µm)
Wild-type
Atxn1154Q/2Q
D.
Aqp4 mRNA (Normalized to 18S)
Gfap mRNA (Normalized to 18S)
Gja1 mRNA (Normalized to 18S)
Kcnj10 mRNA (Normalized to 18S)
C3 mRNA (Normalized to 18S)
Slc1a2 mRNA (Normalized to 18S)
Wild-type
Atxn1154Q/2Q
WT
E.
Astrocyte density (GFAP+ cells/mm²)
GFAP intensity (norm. to aCSF-treated WT littermate)
aCSF
BDNF
Wild-type
Atxn1154Q/2Q

Figure 8.